Designing a robust whole-cell biosensor platform for detection of toxic metals using intein splicing inhibition of *Mycobacterium tuberculosis* SufB protein

Ashwaria Mehra[1†], Ananya Nanda[1,2†], and Sasmita Nayak[1, 3*]

[1] School of Biotechnology, Kalinga Institute of Industrial Technology Deemed to be University, Bhubaneswar, Odisha, India 751024.
[2]Toronto Metropolitan University, 350 Victoria St, Toronto, ON M5B 2K3, Canada
[3] Department of Microbiology, Kalinga Institute of Medical Sciences, Kalinga Institute of Industrial Technology Deemed to be University, Bhubaneswar, Odisha, India 751024
Corresponding Author: sasmita.n@kiitbiotech.ac.in

[†]These authors have contributed equally to this work and share first authorship

Abstract:

Heavy metal contamination has emerged as a persistent environmental and public health challenge. Although existing analytical methods provide high sensitivity, they often require complex instrumentation with limited on-site applications, and generate hazardous waste, raising environmental concerns. At present, whole-cell biosensors provide an empirical alternative, utilizing cellular machinery for sensitive detection of metals. In a relevant context, intein-mediated protein splicing, a spontaneous post-translational process, can be adapted for biosensing by coupling metal-dependent splicing inhibition with whole-cell sensing units. Current research elucidates how toxic metal ions, including cadmium (Cd^{2+}), mercury (Hg^{2+}), chromium (Cr^{3+}), and lead (Pb^{2+}), influence the splicing and N-terminal cleavage reactions of *Mycobacterium tuberculosis* (*Mtb*) SufB precursor protein. While Cd^{2+} and Hg^{2+} significantly attenuated the splicing activity of *Mtb* SufB precursor protein over a concentration range of 25 µM to 2 mM, Pb^{2+} and Cr^{3+} failed to do so. Next, an innovative biosensor platform was designed to detect these metal

ions by utilizing splicing inhibition in metal-sensitive *Mtb* SufB precursor protein within attenuated *Mtb* (H37Ra) cells. Metal-induced splicing inhibition led to loss of viability in H37Ra indicator cells, while specificity of this detection system was confirmed by adding respective metal chelators. Multiplexing and quantitative efficacy of the designed biosensor was evaluated by including known splicing inhibitors like Cu^{2+}, Zn^{2+}, and Pt^{4+} over various concentration range alongside Cd^{2+} and Hg^{2+}. The developed biosensor offers a cost-effective, user-friendly, specific, and sensitive assay that does not require advanced instrumentation facility. It can be employed in standard biological laboratories utilizing whole-cell microorganisms harbouring precursor proteins with metal-sensing intein sequences. This approach holds potential for multiplexing metal screening in environmental and industrial effluents, significantly enhancing toxic metal monitoring capabilities.

Keywords: Whole-cell biosensor, heavy metal ion detection, *Mycobacterium tuberculosis* SufB, intein-based biosensor, protein splicing inhibition.

Heavy metal contamination has emerged as one of the most persistent environmental and public health challenges of the modern era. Over 35 metals have been identified in their ore forms within the Earth's crust, many of which are essential nutrients. Among these, 23 metals are classified as heavy metals due to their high density (>5 g/cm³) and atomic weights (>40.0), indicating their potential for environmental toxicity.[1–3] Human activities have significantly disrupted natural geochemical cycles, causing bioaccumulation and biomagnification through contaminated food, water, or direct exposure, thereby posing serious health risks.[3–7]

Current analytical methods, such as electrothermal atomic absorption spectrometry (ETAAS), inductively coupled plasma-optical emission spectrometry (ICP-OES), high-pressure liquid

50 chromatography combined with ICP-mass spectrometry (HPLC-ICP-MS), hydride generation
51 atomic absorption spectrometry (HGAAS), and X-ray fluorescence spectrometry (XRF), offer
52 excellent sensitivity for detecting metals. Nonetheless, these methods involve complex
53 instrumentation, require skilled operators, generate hazardous waste, contributing further to
54 environmental pollution.[8–11] To overcome these limitations, biosensors have emerged as a
55 promising alternative offering affordability, and long-term operational stability.[8] According to the
56 International Union of Pure and Applied Chemistry (IUPAC), biosensors integrate biological
57 recognition elements directly with transducers to provide precise quantitative data.[12,13] Although
58 enzyme-based electrochemical biosensors have been widely explored, their broader
59 implementation is limited due to poor electron transfer efficiency, and instability, limiting their
60 commercial reusability.[14–20] In comparison, whole-cell biosensors present a more practicable
61 approach by using live cell sensing units, with advantages such as stable signal generation, and
62 scalability. Despite these strengths, declining cell viability causing delayed response time remain
63 challenging.[21–26] Addressing these shortcomings, intein-mediated protein engineering techniques
64 open up new avenues for creating innovative cell-based sensors.[27–30]

65 Inteins are protein splicing elements within precursor proteins that can self-excise via multi-step
66 nucleophilic displacement reactions, to generate active proteins.[31,32] This is a post-translational
67 process that does not require energy sources or cofactors, hence inteins can be seamlessly
68 integrated into biosensor units minimizing interference with sensor cell functionality.[27]
69 Furthermore, intein splicing can be regulated via conditional protein splicing (CPS), in presence
70 of small molecules such as metal ions and metal-based nanoparticles (Table 1).[33–37] For instance,
71 a recent study from our group has examined the splicing and N-terminal cleavage activity of
72 *Mycobacterium tuberculosis* (*Mtb*) SufB precursor protein in the presence of metal ions such as

73 Cu^{2+}, Zn^{2+}, Pt^{4+}, and Fe^{3+}/Fe^{2+}.[38] Prior studies have also reported Zn^{2+} mediated splicing regulation

74 of PI-*Sce* VMA intein, *Mtb* RecA intein, and *Ssp* PCC6803 DnaE split intein.[39,40] Effects of metal

75 ions, such as $Cu^{+/2+}$ and CisPt, have been evaluated on *Mtb* RecA, *Cryptococcus neoformans* Prp8,

76 and *Mycobacterium smegmatis* DnaBi1 intein splicing.[35,36,39,41–46]

77 **Table 1:** Overview of intein-harboring organisms and reported modulation of splicing activity by
78 metal ions

79

Name of Organisms		Intein containing precursor proteins	Metal ions	References
Bacteria	*Mycobacterium tuberculosis*	RecA	Zn^{2+} Cd^{2+} Co^{2+} Ni^{2+} Cu^{+}/Cu^{2+} CisPt	40,42,47,48
	Mycobacterium tuberculosis	SufB	Zn^{2+} Cu^{2+} Pt^{4+} $Fe^{2+/3+}$	38
	Mycobacterium smegmatis	DnaB-intein1 (DnaBi1)	Zn^{2+}	44
	Synechocystis sp. PCC6803	*Ssp* DnaE	Zn^{2+} Cd^{2+}	40
	Oscillatoria limnetica	split DnaE intein	Cu^{2+}	49
	Thermosynechococcus vulcanus	DnaE	Cu^{2+}	49
	Nostoc sp. PCC7120	DnaB	Cu^{2+}	49
Fungi	*Saccharomyces cerevisiae*	PI-*Sce*I VMA	Zn^{2+}	39
	Cryptococcus neoformans	Prp8	Zn^{2+} Cu^{2+} CisPt	36,46

	Cryptococcus gattii	Prp8	CisPt	[46]

80

81 Conditional splicing activity of intein-containing proteins has been widely used to develop
82 biosensors with unique functionalities.[27,50–52] However, a versatile intein-based metal-sensing
83 biosensor, especially for toxic metals ions, is yet to be elucidated. Current research explores how
84 toxic metal ions, like cadmium (Cd^{2+}), mercury (Hg^{2+}), chromium (Cr^{3+}), and lead (Pb^{2+}), affect
85 the splicing and N-terminal cleavage reactions of *Mtb* SufB precursor protein. Furthermore, a
86 whole-cell biosensor system using mycobacterial cells has been developed and evaluated to detect
87 the presence of toxic metal ions via splicing regulation in metal-sensitive precursor protein, *Mtb*
88 SufB.

89 SUF protein complex constitutes a unique pathway for Fe-S cluster assembly in mycobacteria, and
90 its activity is dependent on the splicing of *Mtb* SufB precursor, producing functional SufB
91 protein.[53] Thus, splicing inhibition which blocks the generation of active SufB, can impair
92 mycobacterial growth and viability.[54] In the current work, *in vitro* studies demonstrated significant
93 inhibition of *Mtb* SufB precursor protein splicing in presence of toxic metal ions such as Cd^{2+}, and
94 Hg^{2+} over a concentration range of 25 μM to 2 mM. Further, time-dependent assay revealed that
95 Cd^{2+} and Hg^{2+} could inhibit *Mtb* SufB intein splicing as early as 10 minutes following exposure to
96 the metal ions. Building on this observation, an *in vitro* biosensor platform was designed using
97 H37Ra (an attenuated *Mtb* strain) as metal-indicator cells. Alamar Blue assay performed in a 96-
98 well microtiter plate, detected loss of cell viability in SufB-containing H37Ra cells in presence of
99 toxic metal ions, Cd^{2+} and Hg^{2+}. In contrast, *Mycobacterium smegmatis* (*M. sm*), which expresses
100 an intein-less SufB protein, persisted as healthy, viable cells under similar experimental conditions.

101 Hence, current study highlights the sensitivity of H37Ra-based biosensor platform to detect toxic
102 metal ions via inhibiting the generation of essential protein SufB in mycobacteria. Moreover, the
103 specificity of the biosensor was demonstrated by addition of respective metal chelators which
104 protected mycobacterial cell viability via blocking the splicing-inhibitory roles of the metal ions.
105 Since, Zn^{2+}, Cu^{2+}, and Pt^{4+} are also known inhibitors of *Mtb* SufB splicing, multiplexing and
106 quantitative potential of this platform was validated using various concentrations of these metal
107 ions alongside Cd^{2+} and Hg^{2+}. Thus, this work opens new avenues for developing a reliable and
108 sensitive *in vitro* biosensor platform using whole-cell mycobacteria as biological indicator for
109 toxic metal ions as well as trace metal elements (TME) in the environmental samples. The efficacy
110 of this system lies in its cost-effectiveness, user-friendly design, high specificity, and sensitivity,
111 enabling multiplexed metal detection. It is particularly useful as it can detect toxic metal ions at
112 low concentration (25 μM) within just 10 minutes. Consequently, it can be easily employed in
113 standard biological laboratories equipped with organisms harboring metal-sensitive intein-
114 carrying precursor proteins.

115 **Materials and Methods:**

116 *Protein overexpression and purification* [55–57]

117 Plasmids containing the genes for *Mtb* SufB precursor and *Mtb* SufB splicing inactive (SI) double
118 mutant (Cys1Ala/Asn359Ala) (splicing negative control),[55] both carrying an N-terminal 6X (His)
119 tag, were borrowed from Belfort Lab, SUNY, Albany, USA. The test plasmids were transformed
120 into BL21(DE3) *E. coli* cells (NEB, C2527I), followed by IPTG (500 μM, sigma 367-93-1)
121 induced protein over-expression. Thereafter, lysis buffer (20 mM sodium phosphate, 0.5 M NaCl,
122 pH 7.4) was used to resuspend the bacterial cell pellet and cells were lysed via tip sonicator (Sonics
123 vibra cell VCX-130). The cell lysate was centrifuged at 16500×g for 20 minutes at 4 °C, and the

124 supernatant was discarded. The collected inclusion body (IB) material was then washed three times
125 in lysis buffer via centrifugation (16500×g for 20 minutes at 4 °C). Finally, the IB material was
126 solubilized for protein extraction using 8 M urea (Merck, 1084870500) buffer (20 mM sodium
127 phosphate, 0.5 M NaCl, 8M urea, 10 mM of imidazole, pH 7.4 (MP–biochemicals-288-32-4) and
128 subsequently centrifuged at 16,500×g for 20 minutes at 4 °C to collect the supernatant. Then,
129 solubilized proteins were purified by Ni-NTA affinity column (Ni-NTA His trap, HP GE
130 healthcare life sciences, 17524802).[35,40,48,58,59] Before applying the samples, the columns were
131 equilibrated with binding buffer (20 mM sodium phosphate, 0.5 M NaCl, 8 M urea, 10 mM
132 imidazole, pH 7.4). Following sample loading, the columns were washed multiple times (5 CV)
133 using wash buffer (20 mM sodium phosphate, 0.5 M NaCl, 8 M urea, 40 mM imidazole, pH 7.4).
134 Subsequently, the test proteins were eluted as purified fractions using elution buffer (20 mM
135 sodium phosphate, 0.5 M NaCl, 8 M urea, 500 mM imidazole, pH 7.4). Protein quantification was
136 performed using Bradford reagent.

137 *Refolding assay for Mtb SufB precursor protein*

138 Denatured protein (2.5 μM) in elution buffer was renatured in refolding buffer (20 mM sodium
139 phosphate, 0.5 M NaCl, 0.5 M L-Arginine) containing 2 mM TCEP-HCl (sigma-51805-45-9) for
140 4 hours at 25 ºC in the absence and presence of toxic metal ions.[40,58,59] Gradient assay for toxic
141 metal ions [$CdCl_2$ (SRL-99643), $HgCl_2$ (SRL-25699), $CrCl_3$ (CDH-025702), $PbCl_2$ (SRL-69789)]
142 was performed using varying concentrations of toxic metal ions (2.5 μM to 2 mM). 0h sample was
143 collected before initiation of refolding, and the reaction was abruptly blocked by the addition of
144 loading dye (0.1% bromophenol blue, 50% glycerol, 5% β-mercaptoethanol, 10% SDS, tris 6.8),
145 followed by rapid freezing at −20 ºC. After 4h of protein renaturation, the protein samples were
146 resolved through 4~10% gradient SDS-PAGE, followed by staining with Coomassie brilliant blue

147 R-250 (93473, SRL), and densitometric analysis was performed using GelQuant.NET biochemical
148 solutions software. The splicing and cleavage efficiencies were calculated using the following
149 formulae:

150 $$\%\ of\ splicing = \frac{Total\ splicing\ products\ (LE + I)}{Total\ protein\ (P + LE + I)}\ X\ 100$$

151 $$\%\ of\ N - terminal\ cleavage = \frac{Total\ N - terminal\ cleavage\ products\ (NC + NE)}{Total\ protein\ (P + NC + NE)}\ \text{X}\ 100$$

152 [P: precursor protein, LE: Ligated exteins, I: Intein, NC: N-terminal cleavage product, NE: N-
153 extein]

154 Baseline correction was done using the 0 hours splicing and cleavage value(s). The results were
155 analyzed using one-way ANOVA and plotted using GraphPad Prism version 8 for Windows,
156 GraphPad Software, San Diego, California, USA, www.graphpad.com.

157 *Immunoblotting to identify splicing and N-terminal cleavage protein products*[38]

158 Protein immunodetection was conducted to identify of splicing and N-terminal cleavage reaction
159 products, using anti-6X(His) tag antibodies (Invitrogen, LOT 1902132). After resolution through
160 4~10% gradient SDS-PAGE, the protein products were transferred onto a PVDF membrane
161 (Millipore, IPVH 00010) at 50V for 2 hours at 4 °C. The blot was then blocked with 5% skim milk
162 for 2 hours at room temperature, followed by two washes with 1X TBST. It was incubated with
163 primary anti-6X(His) tag (abgenex -32-6116) at a dilution of 1:5000 at 4 °C for 16 hours. After
164 washing with 1X TBST, the blot was treated with a secondary antibody (anti-mouse; abgenex 11-
165 301) at a dilution of 1:8000 for 2 hours at 37 °C. The N-extein band was detected using a lower
166 dilution of the primary antibody (1:2500) and the secondary antibody (1:6000). Finally, the blot

167 was developed using Enhanced Chemiluminescence substrate (Abcam, ab65628) to visualize the
168 protein bands, and images were captured using in-house ImageQuant^{TM} LAS 500 facility (GE
169 Healthcare). Blots were also developed, using 3, 3'-diaminobenzidine (DAB) (SRL-94524) for
170 visualization of the protein bands.

171 *Spectroscopic and Elemental Profiling of Protein-Metal Interactions*

172 *UV-Visible spectroscopy* [60–62]

173 Denatured proteins were renatured *in vitro* in the presence and absence of toxic metal ions at their
174 respective concentrations for 4 hours, as specified earlier. Subsequently, the treated samples were
175 subjected to UV-visible spectroscopy (Cary 100 UV-Vis Agilent Technology) scanning in the
176 visible region spanning 200-800nm. To rule out the interference from buffer-metal interactions,
177 the refolding buffer (20 mM sodium phosphate, 0.5 M NaCl, 0.5 M L-Arginine) was incubated
178 with metal ions (Cd^{2+}, Hg^{2+}, Cr^{3+}, and Pb^{2+}) at their respective concentrations under similar
179 experimental conditions. This was used as a blank for baseline correction and was scanned
180 alongside each sample. Absorbance versus wavelength plots were generated and analyzed using
181 Origin (Pro) 8.5 software (Version 8.5, OriginLab Corporation, Northampton, MA, USA) to
182 interpret the results.

183 *Tryptophan Fluorescence Spectroscopy*

184 The purified denatured protein (2.5 μM) was allowed to renature in the presence and absence of
185 metals ions (25 μM $CdCl_2$, 500 μM $HgCl_2$, 2 mM $CrCl_3$, and 2 mM $PbCl_2$) under identical
186 experimental conditions. Following 4 hours of refolding, the test samples were analyzed via
187 Fluorescence spectrometry (Cary Eclipse, Agilent Technologies) over a wavelength range of 300-
188 600 nm and at an excitation wavelength of 280 nm.[63] To rule out the buffer-metal interactions, the
189 refolding buffer (20 mM sodium phosphate, 0.5 M NaCl, 0.5 M Arginine) was incubated with

190 metal ions at their respective concentrations at 25 °C for 4 hours and then scanned alongside each
191 treated sample. This served as the blank for baseline correction. The tryptophan fluorescence
192 spectra for the test samples were recorded and analyzed by plotting intensity vs. wavelength using
193 Origin (Pro) 8.5, Version 8.5, from OriginLab Corporation, Northampton, MA, USA.

194 *Inductively coupled plasma-optical emission spectroscopy (ICP-OES) analysis*

195 Following *in vitro* refolding of *Mtb* SufB precursor in the presence of test metal ions, the protein
196 products were resolved through 4~10% SDS-PAGE. The resulting protein bands were visualized
197 with Coomassie brilliant blue R-250. Subsequently, the gel bands for unspliced precursor protein,
198 ligated extein, and intein were excised from the gel for further analysis. Each gel band was then
199 treated with concentrated H_2SO_4 and 30% H_2O_2. Complete dissolution of each sample was
200 achieved by incubating the gel pieces in a 3:1 mixture of concentrated HCl and concentrated HNO_3
201 at 80°C for 4 hours.[64,65] The final volume of the digested solution was adjusted to 50 ml with
202 deionized water and then analyzed by ICP-OES (Perkin-Elner, optima 8300). Prior to analyzing
203 the test samples, respective toxic metal standards were calibrated in the system, and the
204 concentration of bound metal ions was quantified from the standard curve.

205 *In vitro whole-cell (H37Ra) toxic metal biosensor*

206 Different mycobacterial cells [*Mycobacterium tuberculosis* H37Ra strain (ATCC 25177),
207 *Mycobacterium smegmatis* (negative control for SufB intein-less micro-organism, ATCC
208 700084)] were cultured in 7H9 (Middlebrook 7H9 broth medium, M198) supplemented with
209 OADC (Oleic acid, dextrose, and catalase, Himedia-FD018) and allowed to grow separately for 2-
210 3 weeks at 37 ^{0}C. CFU calculations for individual cultures were made by matching the turbidity
211 of the inoculated mycobacterial culture with the McFarland standard (Himedia- R092) against a

212 black background.[66] Different bacterial cells were diluted in sterile saline to a concentration of
213 10^8 CFU/ml. H37Ra cells were incubated with varied concentrations of Cd^{2+} (2.5 µM- 2 mM) and
214 Hg^{2+} (25 µM- 2 mM) in 96-well microtiter plate. Since Cr^{3+} and Pb^{2+} over a test concentration
215 range of 25 µM- 2 mM did not exert any effect on *Mtb* SufB splicing, these metal ions were not
216 tested via the *in vitro* biosensor platform. The plates were sealed and incubated at 37 ºC for 4
217 days. Then, 10% (v/v) solution of Alamar Blue reagent (SRL-42650) was added to each well,
218 followed by incubation at 37 ºC for 12 hrs.[67] Untreated mycobacterial cells grown in 7H9
219 (supplemented with OADC) media were used as a negative control, and Alamar blue reagent alone
220 in 7H9 (supplemented with OADC) media served as a positive control. SufB intein-less organism,
221 *Mycobacterium smegmatis,* was also evaluated under similar conditions and treated as an
222 additional experimental control. After 12 hours of incubation, varied colour changes were noted
223 in different wells, where blue colour indicated dead cells with no viable cell growth, and pink
224 colour correlated to metabolically active live cells. In a similar experimental setup, metal chelators
225 specific for Cd^{2+} (Edetate Calcium Disodium, ECD, Sigma-PHR1510) and Hg^{2+} (meso-2,3-
226 Dimercaptosuccinic acid, DMSA, Sigma-D7881) were added in a ratio of 1:1 (metal: chelator) to
227 determine the specificity of the designed *in vitro* Biosensor platform.

228 Quantitative evaluation of *(H37Ra)-based whole cell toxic metal biosensor*

229 Next, a standard plot was generated by measuring the absorbance of the respective samples at
230 570 nm, with 600 nm as a reference wavelength for quantitative analysis.[67] A wide range of test
231 metal samples (Cd^{2+}, Hg^{2+}) of known concentration were prepared and loaded onto the 96-well
232 plate and Alamar Blue reagent was added under similar experimental conditions. The absorbance
233 of test metal samples was calculated by subtracting the reference absorbance value at 600nm from
234 the absorbance measured at 570nm [$OD_{test} = OD_{570} – OD_{600}$]. Untreated mycobacterial cells grown

235 in 7H9 (supplemented with OADC) media were used as a control for normalization. Using the
236 normalized values, XY scattered plot was obtained where the X axis represented the known
237 concentrations of the test metal ions and the Y axis denoted corresponding absorbance values.
238 Next, to assess the applicability of the standard plot, four test samples (Unknown 1, Unknown 2,
239 Unknown 3, and Unknown 4) containing varying concentrations of $CdCl_2$ and $HgCl_2$ were
240 analyzed under identical experimental conditions. Absorbance values were extrapolated onto the
241 standard curve to calculate the unknown metal ion concentrations, thereby validating the
242 sensitivity and accuracy of the biosensor platform.

243 *Multiplexing evaluation of (H37Ra)-based whole cell metal biosensor*

244 Bacterial cell suspension containing 10^8 CFU/ml of *Mycobacterium tuberculosis* H37Ra were
245 prepared in sterile saline. Cells were incubated with a varied concentration range of $ZnCl_2$ (100
246 µM- 2 mM), $CuCl_2$ (100 µM- 2 mM), $PtCl_4$ (20 µM- 1 mM), $CdCl_2$ (10 µM- 2 mM), and $HgCl_2$
247 (25 µM- 2 mM), in 96-well microtiter plates. The plates were sealed and incubated at 37 ºC for 4
248 days under static conditions. Then, 10% (v/v) solution of Alamar Blue reagent (SRL-42650) was
249 added to each well, followed by incubation at 37 ºC for 12 hrs. Untreated H37Ra cells grown in
250 Middlebrook 7H9 supplemented with OADC media were used as a negative control, while Alamar
251 blue reagent incubated in media alone served as a positive control. SufB intein-less organism,
252 *Mycobacterium smegmatis,* was treated with test metal ions under similar conditions and used as
253 negative experimental control to assess SufB intein-specific response. Post 12 hours of incubation,
254 colour change was noted in the wells, where blue colour indicated dead cells with no viability, and
255 pink colour indicated healthy viable cells.

256 To further ascertain the specificity of the biosensor platform, respective metal-chelating agents
257 were added in separate experimental setup, using a 1:1 molar ratio of metal ions to chelator.
258 Cadmium-specific chelator Edetate Calcium Disodium (ECD; Sigma-PHR1510), mercury-
259 specific chelator meso-2,3-Dimercaptosuccinic acid (DMSA; Sigma-D7881), and a broad-
260 spectrum chelator Ethylenediaminetetraacetic acid (EDTA; HiMedia-MB011), were co-incubated
261 with the respective metal ions under identical experimental conditions. Cell viability was evaluated
262 using Alamar Blue reagent as described earlier.

263 **Results and Discussion**

264 ***Toxic metal ions inhibited Mtb SufB precursor protein splicing***

265 Environmental concentrations of toxic metal ions such as cadmium (Cd^{2+}), mercury (Hg^{2+}),
266 chromium (Cr^{3+}) and lead (Pb^{2+}) have been reported to vary widely. Cd^{2+} concentrations typically
267 ranges from 1 to 10 ppm (approximately 5 μM to 55 μM), Hg^{2+} from 10 to 700 ppm
268 (approximately 4 μM to 3 mM), Cr^{3+} from 5 ppm- 140 ppm (approximately 31 μM – 885 μM) and
269 Pb^{2+} levels from 10 to 50 ppm (approximately 36 μM to 180 μM).[68–83] Earlier studies have shown
270 that metal ion concentrations between 40 μM to 2 mM effectively inhibit intein splicing.[38,84,85]
271 Hence, an *in vitro* gradient assay was performed to evaluate the sensitivity of *Mtb* SufB precursor
272 protein over a selected concentration range of toxic metals ions (2.5 μM to 2 mM) (Figure 1, and
273 Figures S2-S4, Supporting Information). *Mtb* SufB precursor protein (95.98 KDa) follows a
274 canonical intein splicing pathway yielding 40.2 KDa SufB intein and 55.7 KDa ligated exteins
275 (functional SufB protein) as illustrated in Figure S1, Supporting Information.[55] N-terminal
276 cleavage products (65.26 KDa N-terminal cleavage product, 29.9 KDa N-extein) and C-terminal

277 cleavage products (70.12 KDa C-terminal cleavage product, 25.76 KDa C-extein) are the
278 byproducts of *Mtb* SufB splicing reaction. [55]

279 Purified *Mtb* SufB precursor protein was refolded in presence of test metal ions and then resolved
280 through 4~10% gradient SDS PAGE (Figure 1A). Cd^{2+} at 25 μM, and Hg^{2+} at 500 μM of minimum
281 effective concentration (MEC) displayed significant attenuation of splicing and N-terminal
282 cleavage reactions. There was a noticeable accumulation of SufB precursor protein, along with
283 substantial reduction in the splicing products (ligated exteins and intein). Further, Cd^{2+}, and Hg^{2+}
284 at their respective MEC values and higher, induced a near-complete inhibition of N-terminal
285 cleavage reaction and the products (N-terminal cleavage product and N-extein) (Figure 1A).
286 However, Cr^{3+} and Pb^{2+} failed to induce any effect on *Mtb* SufB splicing or cleavage reactions
287 across the test concentration range (Figure 1A). Resultant protein products were further confirmed
288 via western blot using anti-6X(His) tag antibody (Figure S2, Supporting Information).
289 Densitometric analysis revealed a 12.52-fold ($p<0.0001$) reduction in splicing efficiency and an
290 18.7-fold ($p<0.0001$) reduction in N-terminal cleavage efficiency with 25 μM Cd^{2+} [Figure 1B (i)
291 and C (i)]. Similarly, treatment with 500 μM Hg^{2+} resulted in an 8-fold ($p < 0.0001$) reduction in
292 splicing and a 7.8-fold ($p < 0.0001$) decrease in N-terminal cleavage efficiency [Figure 1B (ii) and
293 1C (ii)]. No significant alterations in SufB splicing or N-terminal cleavage products were obtained
294 in presence of Cr^{3+} or Pb^{2+} (Figure 1B and 1C). All the test metal ions at a lower concentration
295 range (2.5 μM- 10 μM) failed to exert any significant effect on the SufB splicing reactions (Figures
296 S3 and S4, Supporting Information). In order to rule out the possibility of precursor protein
297 degradation by test metal ions, *in vitro* refolding assays were also conducted using splicing inactive
298 (SI) *Mtb* SufB double mutant (C1A/N359A) under similar experimental conditions (25 μM Cd^{2+},
299 500 μM Hg^{2+}, 2 mM Cr^{3+}, and 2 mM Pb^{2+}). Since Cr^{3+}, and Pb^{2+} showed no regulatory effects,

300 highest test concentration range for both were included in the above study. SDS-PAGE and
301 subsequent western blot analysis using anti-6X(His) tag antibodies confirmed the absence of
302 protein degradation products (Figures S2B, Supporting Information).

303

304
305
306
307
308
309
310
311
312

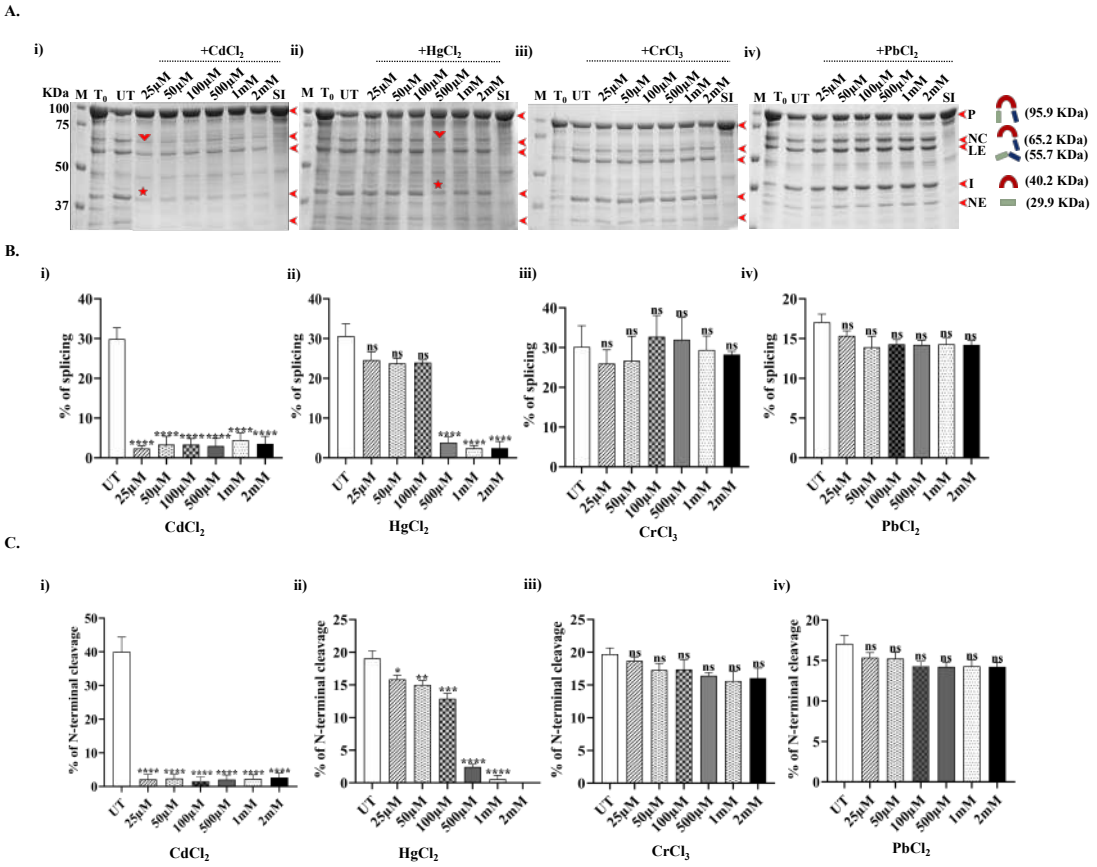

313

314 **Figure 1. Gradient assay to determine the minimum effective concentration (MEC) of toxic**
315 **metal ions on splicing and N-terminal cleavage reactions of *Mtb* SufB precursor protein. (A)**
316 Following *in vitro* refolding of *Mtb* SufB precursor protein in the presence of (i) $CdCl_2$, (ii) $HgCl_2$,
317 (iii) $CrCl_3$, and (iv) $PbCl_2$ at varied concentrations (25 μM-2 mM), resultant products were resolved
318 through 4~10% gradient SDS-PAGE. Lane 1: Protein ladder; Lane 2 (T_0): splicing and N-terminal
319 cleavage reactions at 0 h; Lane 3 (UT): splicing and N-terminal cleavage products of untreated
320 protein sample; Lanes 4-9: splicing and N-terminal cleavage products resulting in the presence of
321 different toxic metal ions at different concentrations (25 μM-2 mM). Lane 10 (SI): splicing
322 inactive SufB double mutant (C1A/N359A) is used as a negative control for splicing. **(B) and (C)**

323 Bar graphs demonstrating splicing and N-terminal cleavage efficiency of *Mtb* SufB precursor
324 protein in the presence and absence of different toxic metal ions. A statistically significant
325 difference in splicing and N-terminal cleavage reaction was observed for B (i) and C (i) $CdCl_2$,
326 starting with 25 μM, and B (ii) and C (ii) $HgCl_2$ at 500 μM concentrations, respectively. For $CrCl_3$
327 [B (iii) and C (iii)], and $PbCl_2$ [B (iv) and C (iv)], no significant difference in splicing and N-
328 terminal cleavage reaction were observed between untreated and metal-treated samples. Graphs
329 were plotted after densitometric analyses using GelQuant.Net biochemical solutions. All the
330 experiments were performed in triplicate, and error bars represent (±1) SEM from 3 independent
331 sets of experiments. The data shown in Figures 1B, and 1C are extracted from Figure 1A. M:
332 Prestained protein molecular weight ladder, P: Precursor, NC: N-terminal cleavage product, LE:
333 Ligated extein, I: intein, NE: N-extein.

334

335 Further, a time-dependent splicing assay was performed to examine *Mtb* SufB splicing and
336 cleavage activity over a period of 10 min- 4 hr., elucidating remarkable inhibitory roles of Cd^{2+}
337 (25 μM) and Hg^{2+} (500 μM) as early as 10 minutes (Figure S5, Supporting information). Next, to
338 evaluate the possible physical interaction between *Mtb* SufB protein and the metal ions, a series of
339 experiments were conducted, as shown in the upcoming section. For the said interaction study, the
340 MEC for Cd^{2+}, Hg^{2+} (25 μM, 500 μM, respectively), which inhibited *Mtb* SufB splicing was
341 selected. Since, Cr^{3+}, and Pb^{2+} did not exhibit any such regulatory activity, highest value of the test
342 concentration range (2 mM) was chosen to examine possible interaction with SufB protein.

343 **Protein~ metal interaction study**

344 ***UV-Visible spectroscopic analysis***

345 Biomolecules such as proteins exhibit a strong affinity for metal ions, which can critically
346 influence their structure and function.[86] Prior studies have demonstrated that toxic metal ions such
347 as Cd^{2+}, Hg^{2+}, Cr^{3+}, and Pb^{2+} can interact with calcium and zinc-binding sites in proteins, thereby
348 influencing their biological activity.[87,88] UV-visible spectroscopic analysis was conducted to
349 investigate the interaction between the *Mtb* SufB precursor protein and toxic metal ions under
350 treated and untreated conditions. Absorbance spectra for *Mtb* SufB protein were recorded over

351 200-800 nm range at 25 °C (Figure S6, Supporting Information). A characteristic absorbance peak
352 near 280 nm was detected, primarily attributable to aromatic residues such as tryptophan and
353 tyrosine.[89,90] Upon treatment with Cd^{2+}, an increase in absorbance intensity was noted, suggesting
354 an alteration in conformation due to metal coordination (Figure S6 (i), Supporting Information).
355 Previous studies have mentioned that enhanced absorbance may result from the interaction
356 between Cd^{2+} and electron-donating groups such as amide, imidazole, and amine.[61,91,92] Likewise,
357 samples treated with Hg^{2+} also exhibited an increase in absorbance intensity (Figure S6 (ii),
358 Supporting Information). This enhancement is likely attributed to the strong affinity of Hg^{2+} for
359 nucleophilic functional groups, particularly the sulfhydryl (–SH) groups of cysteine residues.[93,94]
360 Although there were sharp increments in absorbance peak following interaction of $Cr^{3+}$and Pb^{2+}
361 with *Mtb* SufB, they failed to exert any effects on SufB splicing reactions as shown earlier (Figure
362 1). Moreover, a strong buffer-Pb^{2+} interaction was observed from the results, which may have
363 weakened likely interaction with the protein. Although prior works have shown interaction of Cr^{3+},
364 and Pb^{2+} with thiol, glutathione groups within protein structure including oxygen, nitrogen, and
365 sulfur containing amino acids, [7,95,96] current work could not detect any effects of these metal ions
366 on *Mtb* SufB splicing activity (Figure S6 (iii and iv), Supporting Information). To further
367 substantiate such interactions, tryptophan fluorescence spectroscopy was performed, as explained
368 in the forthcoming section.

369 ***Tryptophan Fluorescence spectroscopy reveals metal-induced conformational changes in Mtb***
370 ***SufB***

371 Tryptophan fluorescence spectroscopy is a widely utilized technique for monitoring protein
372 conformational alterations and assessing their local structural dynamics upon interaction with
373 ligands or other macromolecules.[97] Among the intrinsic fluorophores in proteins, aromatic amino

374 acids—tryptophan (Trp), tyrosine (Tyr), and phenylalanine (Phe)—contribute to fluorescence,
375 with tryptophan exhibiting the highest molar absorptivity (1614 cm^{-1}/M) and a characteristic
376 emission peak typically in the range of 340–350 nm.[98] The indole ring of Trp is primarily
377 responsible for this emission and dominates the fluorescence profile over Tyr and Phe. Changes in
378 the microenvironment of tryptophan residues, such as those caused by ligand binding, protein
379 folding, or metal interaction, can lead to measurable shifts in fluorescence intensity and/or
380 emission maxima.[97,99]

381 Altogether, 13 Trp residues are present, spanning the entire sequence of *Mtb* SufB precursor
382 protein, with 5 Trp in N-extein, 5 Trp in Intein, and 3 Trp in the C-extein region.[38] Upon treatment
383 with Cd^{2+} (25 μM), an increase in fluorescence intensity was observed (Figure S7 (i), Supporting
384 Information), likely attributable to conformational rearrangements arising from interactions
385 between Cd^{2+} and functional groups such as amide, imidazole, and amine moieties within the
386 protein matrix.[61,91,92] These interactions may have led to reduced solvent exposure of Trp residues
387 or stabilized a more rigid protein conformation, which can enhance fluorescence emission. [61,100]
388 In contrast, Hg^{2+} (500 μM) treated samples displayed a significant quenching of Trp fluorescence
389 (Figure S7 (ii), Supporting Information). This effect is consistent with previous studies indicating
390 that mercury ions interact strongly with aromatic systems through cation–π interactions,
391 particularly with the indole ring of tryptophan, thereby reducing fluorescence emission.[101] Cr^{3+}
392 (2mM) exposure resulted in a slight increase in fluorescence intensity (Figure S7 (iii), Supporting
393 Information), potentially due to the preferential binding of Cr^{3+} to carboxyl groups, which may
394 induce localized structural stabilization without extensive perturbation of the overall tertiary
395 structure.[102,103] In case of Pb^{2+} (2 mM), a decrease in fluorescence intensity was observed (Figure
396 S7 (iv), Supporting Information). This observation is supported by previous literature, where Pb^{2+}

397 interacts with hydroxy, amino, and sulfhydryl groups, leading to partial protein unfolding and
398 increased solvent accessibility of Trp residues, thereby promoting fluorescence quenching.[104,105]
399 Although Cr^{3+}, Pb^{2+} have displayed possible alteration in protein conformation, they failed to
400 regulate *Mtb* SufB splicing and cleavage reactions, likely due to lack of any effect on protein active
401 site. Next, ICP-OES analysis was conducted to further ascertain potential interaction between test
402 metal ions and protein backbone, as described in the following section.

403 ***ICP-OES detects metal ions bound to SufB precursor and spliced out protein fractions***

404 ICP-OES is a sensitive analytical technique capable of detecting trace metal concentrations by
405 measuring the characteristic emission of photons from the excited atoms and ions as they return to
406 their ground state.[106] During *in vitro* protein refolding experiment, specific concentrations of Cd^{2+}
407 (25 μM = 4.583 μg/ml), Cd^{2+} (500 μM = 91.66 μg/ml), Hg^{+2} (500 μM = 135.76 μg/ml), Cr^{+3} (2
408 mM = 361.72 μg/ml), and Pb^{+2} (2 mM = 556.2 μg/ml) were added to the respective reaction
409 mixture. ICP-OES analysis of the metal-bound protein fractions revealed detectable levels of Cd^{2+}
410 (2 ppb ~ 0.002 μg/ml), Hg^{2+} (5 ppb, ~0.005 μg/ml), and Cr^{3+} (80 ppb, ~0.08 μg/ml) bound to the
411 unspliced *Mtb* SufB precursor protein (Table 2). These findings indicate a direct and quantifiable
412 physical interaction between the toxic metal ions and the *Mtb* SufB precursor protein, which may
413 underlie the observed inhibition of splicing and N-terminal cleavage reactions. Further, measurable
414 interactions were observed between the test metal ions and various splicing products (ligated extein
415 and intein) (Table 2). Cd^{2+} addition to SufB protein sample at 25 μM concentration yielded
416 negative results, while increasing the concentration to 500 μM led to positive data. At lower
417 concentrations of Cd^{2+} (25 μM), the metal content in the protein fraction was possibly below the
418 instrument's limit of detection (LOD) and limit of quantification (LOQ), resulting in negative
419 readings. Although ICP-OES is capable of detecting metal concentrations at the ppb level, practical

420 detection limits are influenced by matrix complexity and background interference, often resulting
421 in quantification thresholds closer to the ppm range.[107–109] Although 80 ppb (0.08 µg/ml) of Cr^{3+}
422 was bound to the unspliced precursor (Table 2), it failed to exert any visible effects on *Mtb* SufB
423 splicing reactions. No bound form of metal ions was detected in Pb^{2+} treated samples, even at 2
424 mM concentration, consistent with no visible effect on *Mtb* SufB splicing.

425 **Table 2:** Quantitative elemental detection via ICP-OES analysis: Measurable concentration of
426 metal ions (Cd^{2+}, Hg^{2+}, Cr^{3+}, and Pb^{2+}) were identified bound to *Mtb* SufB precursor and splicing
427 products. P: Precursor, LE: Ligated extein, I: Intein.

428

429

Metal ions	Treated concentration	Concentration (µg/ml)	ICP-OES values (ppb)	Equivalent Concentration (µg/ml)
Cadmium (Cd^{2+})	25µM	4.583	P: -9 LE: -5 I: -8	P: -0.009 LE: -0.005 I: -0.008
Cadmium (Cd^{2+})	500 µM	91.66	P: 2 LE: 18 I: 1	P: 0.002 LE: 0.018 I: 0.001
Mercury (Hg^{2+})	500 µM	135.76	P: 5 LE: 3 I: 5	P: 0.005 LE: 0.003 I: 0.005
Chromium (Cr^{3+})	2mM	361.72	P: 80 LE: 83 I: 90	P: 0.08 LE: 0.083 I: 0.09
Lead (Pb^{2+})	2mM	556.2	P: -17 LE: -5 I: -73	P: -0.017 LE: -0.005 I: -0.073

430
431
432
433
434
435
436
437

438 Collectively, the gradient and time-dependent splicing assays, along with protein~metal
439 interaction studies, suggested possible interaction of Cd^{2+} and Hg^{2+} with *Mtb* SufB precursor

440 protein, thereby attenuating the splicing and N-terminal cleavage efficacy. These mechanistic
441 insights led to the development of an *in vitro* whole-cell biosensing platform utilizing H37Ra (*Mtb*
442 attenuated strain) cells, as the metal indicator to detect metal ions.

443 Fe-S clusters are essential cofactors for distinct metabolic pathways and cellular processes such as
444 respiration, metabolism, DNA replication and repair, antibiotic resistance and persistence under
445 oxidative and nitrosative stress conditions.[110–112] SUF complex offers the sole pathway for Fe-S
446 cluster biogenesis in mycobacteria, and its activity relies on generation of functional SufB via
447 protein splicing.[53,54] Besides, there are earlier reports on loss of cellular viability as a result of SufB
448 splicing inhibition within mycobacteria.[37,38,46,48,57,59,113–116] Since, toxic metal ions like of Cd^{2+}
449 and Hg^{2+} were shown to inhibit *Mtb* SufB splicing and N-terminal cleavage activity, an attenuated
450 strain of *Mtb* (H37Ra) was used as the whole-cell viability indicator for these metal ions.

451 **H37Ra- based whole-cell biosensor detects toxic metal ions**

452 Cell-based biosensors are gaining interest as a screening platform for biologically active molecules
453 due to their ability to monitor the cellular functions and interactions with targets in their natural
454 environment.[117,118] Often, they are fabricated as genetically encoded biosensors using native
455 receptors or enzymes as molecular recognition elements in living cells.[26] Current work explores
456 the use of whole-cell mycobacteria (H37Ra)-based biosensor to detect toxic metal ions like Cd^{2+}
457 and Hg^{2+}. An *in vitro* 96-well plate assay was developed using Alamar Blue reagent, employing
458 *Mtb* (H37Ra) cells as the sensing component, and *M. sm* cells as the SufB intein-less cellular
459 control.[55,115,119] *M. sm* carries three intein-bearing proteins: DnaB, which contains two inteins
460 (DnaBi1 and DnaBi2), as well as GyrA and PhoH.[44,57] Although splicing regulation has been
461 reported for DnaBi1 helicase, studies on the DnaBi2, PhoH, GyrA inteins splicing have not been

462 explored yet. DnaBi1 splicing is regulated by zinc and oxidative stressors;[44,57] however, its helicase
463 function can be compensated by other cellular helicases.[120–122]

464 Alamar Blue reagent is a non-toxic, resazurin-based solution that functions as an indicator for cell
465 viability.[67,123] The blue-coloured non-fluorescent resazurin (7-hydroxy-3H-phenoxazin-3-one 10-
466 oxide) gets reduced to resorufin (7-hydroxy-3H-phenoxazin-3-one, pink coloured compound) by
467 mitochondrial reductase in metabolically active cells.[124] In a comparative study, non-viable H37Ra
468 were visualized in presence of Cd^{2+} and Hg^{2+}, whereas persistence of viable *M. sm* cells during the
469 metal-interaction process highlighted the absence of metal sensing SufB precursor protein.
470 Untreated H37Ra cells grown in 7H9 (supplemented with OADC) media, and Alamar Blue reagent
471 alone in 7H9 (supplemented with OADC) media, served as the negative and positive controls for
472 the study respectively.

473 Figure 2 (i) is a schematic representation of *in vitro* 96-well plate-based biosensor platform
474 containing *Mtb* H37Ra cells (indicator organisms) incubated with varied concentrations of Cd^{2+}
475 (2.5 μM -2 mM) and Hg^{2+} (25 μM -2 mM). The test concentration range for the metal ions were
476 chosen based on the positive results obtained during *in vitro* splicing analyses (Figure 1, Figures
477 S2-S4, Supporting Information). For a baseline correction, H37Ra cells were grown in the absence
478 of toxic metal ions (negative control). SufB intein-less, *M. sm* cells were used as additional
479 experimental control. Unlike *Mtb* H37Ra cells, the growth and viability of the *M. sm* cells are
480 independent of SufB intein splicing, and any loss of cell viability indicates metal toxicity. Figure
481 2 (ii) shows that the indicator cells (H37Ra) incubated in the presence of lower concentration of
482 Cd^{2+} (2.5-10 μM) did not lose cell viability. All the cells were metabolically active and converted
483 resazurin (blue) to resorufin (pink), since Cd^{2+} at these concentration (2.5-10 μM) didn't affect
484 SufB splicing activity, generating active SufB protein (Figure S3 (i), Supporting Information).

485 H37Ra cells incubated in presence of 25 and 50 μM of Cd^{2+}, displayed purple colour indicating a
486 partial loss of cell viability, underscoring 25 μM as the minimum inhibitory concentration (MIC).
487 Cells incubated with Cd^{2+} at a concentration range of 100 μM- 2 mM, retained blue colour,
488 indicating complete loss of cell viability. These results correlated to inhibition of splicing and N-
489 terminal activity of *Mtb* SufB in presence of Cd^{2+} over a concentration of 25 μM - 2 mM (Figure
490 1).

491 Next, cells incubated in the presence of 25 μM and 50 μM of Hg^{2+} resulted in healthy viable (pink)
492 cell population, whereas cells in the presence of 100 μM Hg^{2+} exhibited purple colour, highlighting
493 partial loss of cell viability at MIC value. Over rest of the concentration range for Hg^{2+} (500 μM-
494 2 mM), non-viable (blue) cells were noticed. These results were supported by SufB splicing
495 attenuation by Hg^{2+} (500 μM-2 mM), while a lower concentration (2.5 μM-10 μM) Hg^{2+} failed to
496 exert any such effects (Figure 1, Figure S4, Supporting Information). Although 100 μM of Hg^{2+}
497 didn't influence SufB splicing, the N-terminal cleavage reaction was reduced significantly,
498 marking this as the MIC value with partial loss of cell viability. Summarizing, persistence of blue
499 colour in the presence of Cd^{2+} (100 μM until 2 mM), and Hg^{2+} (500 μM until 2 mM) may be
500 correlated to complete loss of H37Ra viability due to inhibition of *Mtb* SufB splicing and N-
501 terminal cleavage reactions (Figure 1). These results suggest the potential of mycobacterial
502 (H37Ra) cells as the biological indicator for toxic metal detection.

503

504

505

506

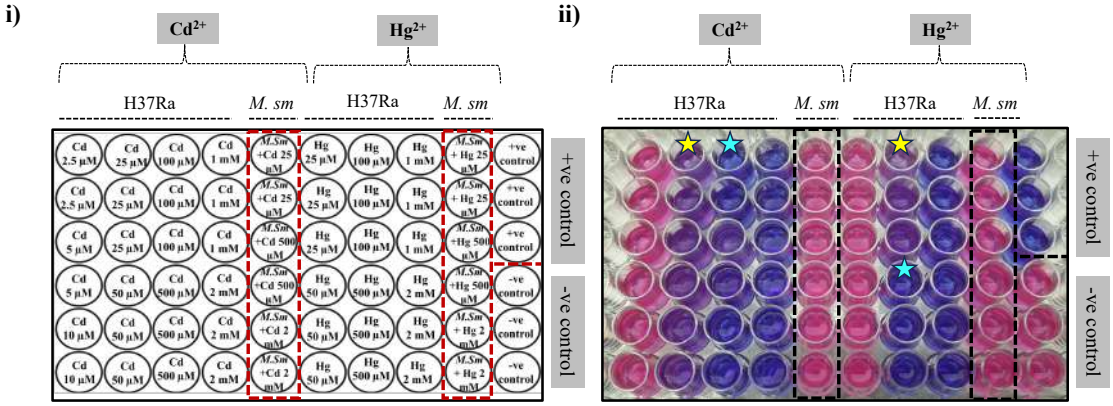

Figure 2. 96-well plate-based biosensor assay demonstrating whole cell mycobacteria (*Mtb* H37Ra strain) as the biological indicator for toxic metal ions (Cd^{2+} and Hg^{2+}) (i) Schematic representation of 96 well plate-based Biosensor platform. (ii) H37Ra cells (10^8 CFU/ml) were seeded in the presence of varied concentration ranges of $CdCl_2$ (2.5 µM- 2 mM) and $HgCl_2$ (25 µM- 2 mM), respectively. Cells incubated in the presence of $CdCl_2$ (2.5 µM- 10 µM) and $HgCl_2$ (25 µM- 50 µM) were pink in colour indicating healthy viable cells resisting the splicing inhibitory effect of the metal ions. In contrast, cells exposed to $CdCl_2$ (25 µM and 50 µM) and 100 µM of $HgCl_2$ displayed purple colour suggesting partial loss of cell viability. Cells incubated with 100 µM-2 mM of $CdCl_2$ and 100 µM- 2 mM of $HgCl_2$ remained blue, suggesting complete loss of viable cell population. For a baseline correction, test organisms were allowed to grow in the absence of toxic metal ions and denoted as live cell control (negative control). SufB intein-less organism *Mycobacterium smegmatis (M. sm)* was used as additional experimental control and treated under similar conditions. *M. sm* cells exhibited pink colour across a varied range of toxic metal ions, suggesting their cell viability as an intein-independent phenomenon. The experiments were performed in triplicates to confirm the reproducibility of data. Cyan stars- complete loss of viability (blue) & Yellow stars- partial loss of viability (purple).

Next, a quantitative analysis for the toxic metal ions was performed by measuring the absorbance of Alamar Blue reagent at 570 nm with 600 nm as a reference wavelength.[67] Metal samples of known concentrations were prepared and loaded on to the 96-well plate and treated with Alamar Blue reagent under optimised experimental conditions [Figures 3 (i)-(iv)]. A standard graph was generated by plotting the absorbance values of Alamar reagent vs the known concentrations of test

535 metal ions (Cd^{2+} and Hg^{2+}) [Figures 3 (v) and (vi)]. Subsequently, a linear regression analysis was
536 performed to determine the equation of the line, expressed as y = mx + c. To further validate the
537 standard plot, unknown samples with varying concentrations of Cd^{2+} ions and Hg^{2+} ions were
538 prepared (Materials and Methods). Absorbance values of the unknown samples were extrapolated
539 onto standard graph to determine the concentrations of Cd^{2+} and Hg^{2+} (Figures 3 (v), (vi) and Table
540 S1, Supporting Information). Unknown samples with concentration higher than the standard range
541 may be adjusted via dilution, or the standard calibration plot may be extended to higher
542 concentration ranges.[125] However sample concentration at a value lower than the standard range
543 cannot be determined accurately possibly due to no effect on intein splicing and hence no loss of
544 cell viability.

545

546
547
548
549
550
551

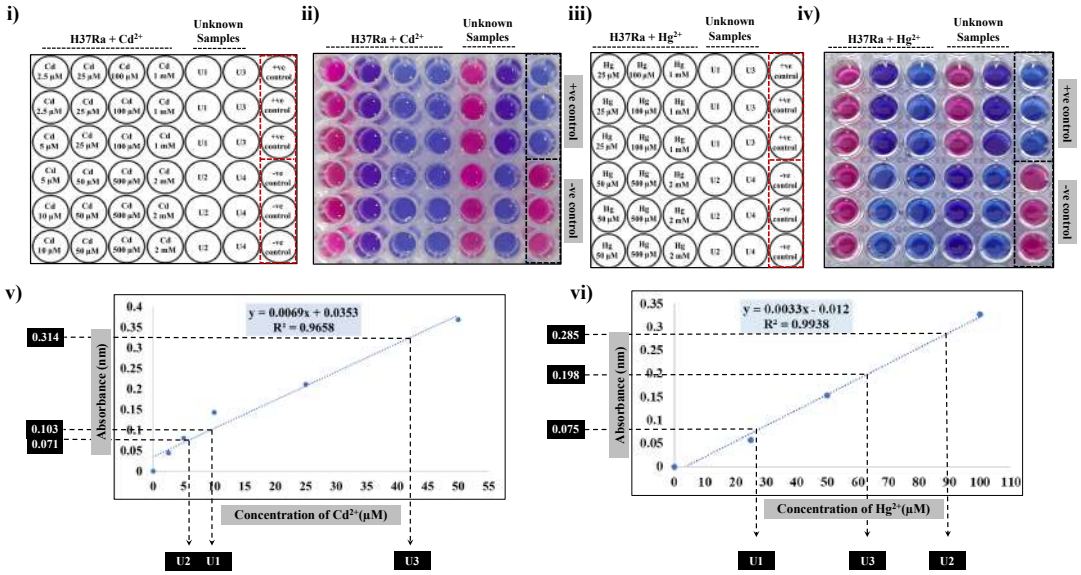

552

553 **Figure 3. Standard curve for quantitative determination of Cd^{2+} and Hg^{2+} concentrations.**
554 (i), and (iii) Schematic representations of H37Ra-based Biosensor platform to detect $CdCl_2$ and
555 $HgCl_2$. (ii), and (iv) *Mtb* H37Ra cells were grown in presence of varied concentration of $CdCl_2$
556 and $HgCl_2$. To establish a baseline, test organisms were allowed to grow in absence of toxic metal
557 ions (live cell or negative control). (v), and (vi) The absorbance values of the Alamar Reagent

558 solutions were plotted along the y-axis and the known concentrations of Cd^{2+} and Hg^{2+} were
559 plotted along the x-axis. A linear regression analysis was conducted to obtain the equation for the
560 line, and used to determine the concentration of unknown samples. The experiments were
561 performed in triplicates to confirm the reproducibility of data.

562

563 Next, to elucidate the specificity of the designed biosensor platform, Cd^{2+}- and Hg^{2+}- specific
564 metal chelators, Edetate Calcium Disodium (ECD), and meso-2,3-Dimercaptosuccinic acid
565 (DMSA) were incubated alongside the test samples.[126–131] Figure 4 (i) is a schematic representation
566 of the *in vitro* biosensor platform, where indicator mycobacterial cells were exposed to Cd^{2+} and
567 Hg^{2+}, in presence of Cd^{2+}-specific chelator, ECD. Figure 4 (ii) demonstrates that ECD effectively
568 resisted Cd^{2+}- induced loss of viability, resulting in healthy cells that transformed resazurin (blue)
569 to resorufin (pink). Conversely, ECD failed to restore viability of Hg^{2+} treated cells, where
570 inhibition of SufB splicing, rendered non-viable (blue) cells. Next, mycobacterial cells were
571 subjected to varying concentrations of Cd^{2+} and Hg^{2+}, supplemented with metal chelator DMSA
572 (Hg^{2+} specific) [Figure 4 (iii) and (iv)]. Hg^{2+} treated H37Ra cells remained viable in presence of
573 DMSA, while Cd^{2+} continued its inhibitory effect on SufB splicing inducing non-viable (blue)
574 cells. These observations affirmed the specificity of the designed biosensor platform to detect
575 toxic metal ions Cd^{2+} and Hg^{2+}.

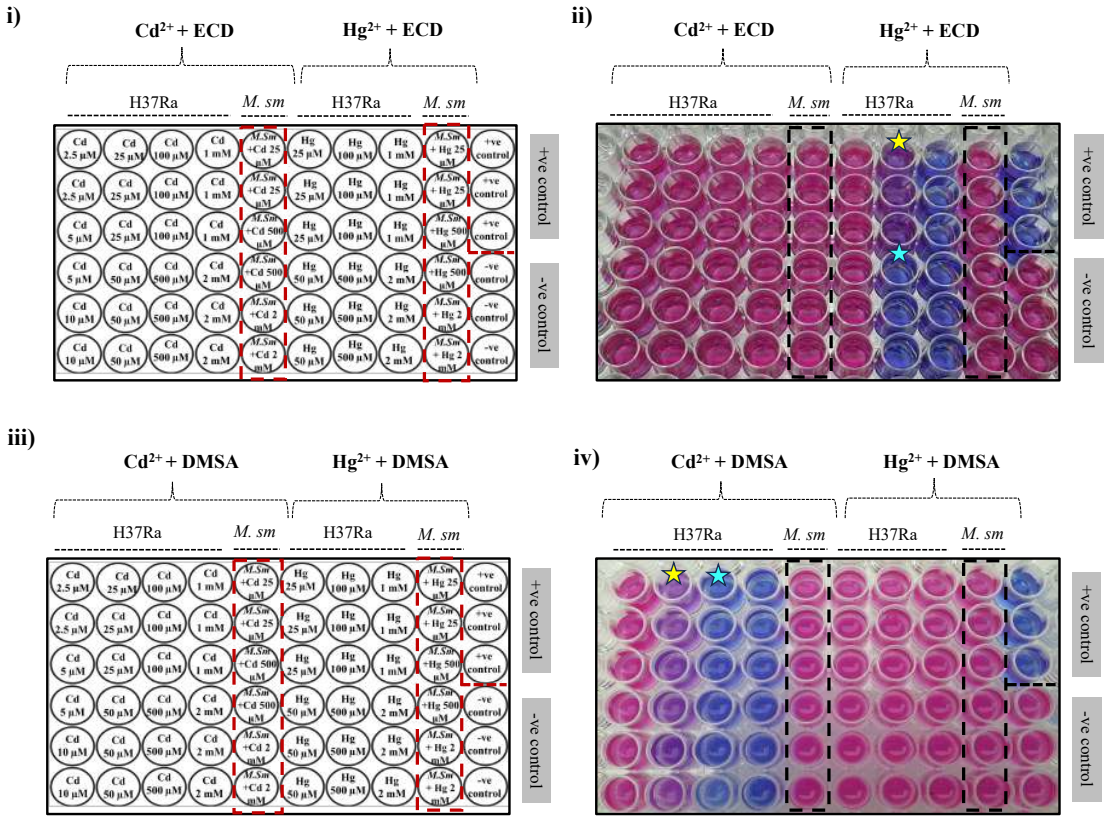

Figure 4. Determination of the specificity of *Mtb* H37Ra-based biosensor platform using metal chelators. (i) Schematic representation of the biosensor platform including Cd^{2+} specific metal chelator (ECD) (ii) *Mtb* H37Ra cells (10^8 CFU/ml) were allowed to grow in presence of varied concentration range of $CdCl_2$ and $HgCl_2$, along with ECD (1:1 ratio). ECD reversed the inhibitory effect of Cd^{2+} inducing viable (pink) cells, whereas the effect of Hg^{2+} persisted (iii) Schematic representation of the biosensor platform including Hg^{2+} specific metal chelator (DMSA). (iv) *Mtb* H37Ra cells (10^8 CFU/ml) were allowed to grow in the presence of varied concentration ranges of $CdCl_2$ and $HgCl_2$, including DMSA in the ratio 1:1. DMSA blocked the inhibitory effect of Hg^2, rendering pink viable cells, whereas the effect of Cd^{2+} persisted. For a baseline correction, H37Ra cells were grown in the absence of toxic metal ions as the live cell control. SufB intein-less organism *Mycobacterium smegmatis (M. sm)* was used as additional experimental control and treated under similar conditions. *M. sm* cells exhibited pink colour across a varied range of toxic metal ions, suggesting their cell viability as an intein-independent phenomenon. The experiments were performed in triplicates to confirm the reproducibility of data. Cyan stars- complete loss of viability (blue) & Yellow stars- partial loss of viable cells (purple). ECD: Edetate Calcium disodium, DMSA: Meso-2,3-Dimercaptosuccinic acid.

602

603 Next for a multiplex metal screening process, the efficacy of the platform was assessed in presence
604 of known splicing inhibitors Zn^{2+} (100 μM-2 mM), Cu^{2+} (100 μM-2 mM), Pt^{4+} (20 μM-1 mM)
605 along with Cd^{2+} (10 μM-2 mM) and Hg^{2+} (25 μM-2 mM) (Figure 5).[38] Baseline correction was
606 achieved by growing H37Ra cells in the absence of toxic metal ions (negative control), while SufB
607 intein-less *M. sm* cells served as additional experimental control. Cells treated with 100 μM $ZnCl_2$
608 and $CuCl_2$, 20 μM $PtCl_4$, 10 μM $CdCl_2$, and 25 μM $HgCl_2$, turned pink in colour, indicating intact
609 viability. At intermediate concentrations, 600 μM of $ZnCl_2$ and $CuCl_2$, 40 μM $PtCl_4$, 25 μM $CdCl_2$,
610 and 100 μM $HgCl_2$, a transition from blue to purple colour was observed, suggesting partial loss
611 of cell viability. Complete loss of viability was noted at higher concentration range, for $ZnCl_2$ and
612 $CuCl_2$ (800 μM- 2 mM), $PtCl_4$ (80 μM- 1 mM), $CdCl_2$ (100 μM- 2 mM), and $HgCl_2$ (500 μM- 2
613 mM) (Figure 5 ii). Dead non-viable cells induced by Zn^{2+}, Cu^{2+}, and Pt^{4+} may be correlated to
614 inhibition of *Mtb* SufB splicing and N-terminal cleavage reactions as published earlier.[38] In
615 contrast, SufB intein-less organism (*M. sm*) remained viable (pink) under similar experimental
616 conditions, suggesting cell viability as a splicing independent phenomenon. These observations
617 may also be used to rule out metal toxicity on cell viability over the test concentration range.

618

619

620

621

622

623

624

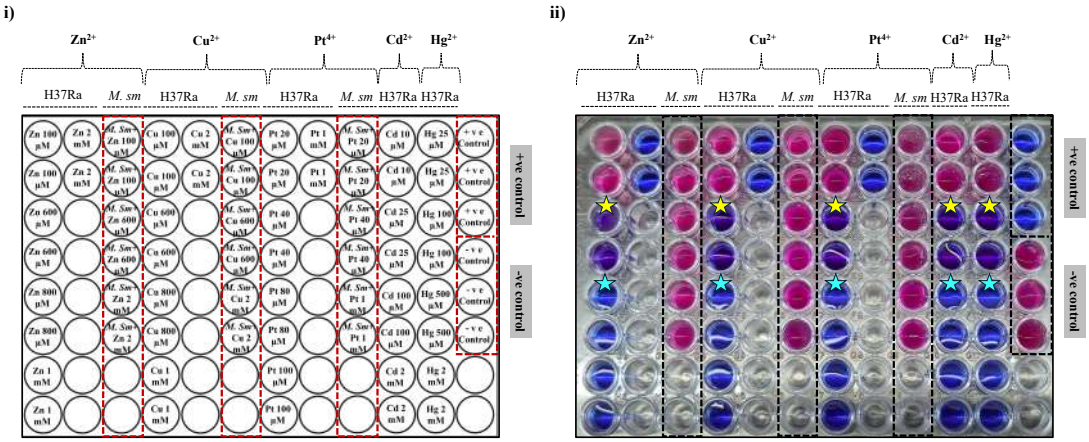

Figure 5. Evaluation of *Mtb* H37Ra-based biosensor platform for high-throughput and multiplex detection of trace metal elements and toxic metal ions (Zn^{2+}, Cu^{2+}, Pt^{4+}, Cd^{2+}, and Hg^{2+}). (i) Schematic representation of the multiplexing biosensor platform. (ii) H37Ra cells (10^8 CFU/ml) were allowed to grow in the presence of $ZnCl_2$ (100 µM- 2 mM), $CuCl_2$ (100 µM- 2 mM), $PtCl_4$ (20 µM- 1 mM), $CdCl_2$ (10 µM- 2 mM) and $HgCl_2$ (25 µM- 2 mM), respectively. Cells incubated with 100 µM of $ZnCl_2$ and $CuCl_2$, 20 µM of $PtCl_4$, 10 µM of $CdCl_2$ and 25 µM of $HgCl_2$ were pink in colour indicating healthy viable cells. In contrast, cells exposed to 600 µM of $ZnCl_2$ and $CuCl_2$, 40 µM of $PtCl_4$, 25 µM of $CdCl_2$ and 100 µM of $HgCl_2$ turned purple in colour suggesting partial loss of cell viability, whereas cells exposed to 600 µM- 2 mM of $ZnCl_2$ and $CuCl_2$, 80 µM- 1 mM of $PtCl_4$, 100 µM- 2 mM of $CdCl_2$ and 500 µM- 2 mM of $HgCl_2$ remained blue in colour suggesting complete loss of viable cell population. For a baseline correction, H37Ra cells were grown in the absence of toxic metal ions as the live cell control (negative control). SufB intein-less organism *Mycobacterium smegmatis (M. sm)* was used as additional experimental control and treated under similar conditions. *M. sm* cells exhibited pink colour across a varied range of toxic metal ions, suggesting their cell viability as an intein-independent phenomenon. The experiments were performed in triplicates to confirm the reproducibility of data. Cyan stars- complete loss of viability (blue) & Yellow stars- partial loss of viability (purple).

Further assessment of the multiplexing biosensor platform was done by employing metal-specific chelators along with the metal-treated samples. The Cd^{2+}-specific chelator ECD and Hg^{2+}-specific chelator DMSA were tested alongside the broad-spectrum metal chelator EDTA. Figure 6 (i) is a

656 schematic representation of the *in vitro* biosensor platform, where indicator mycobacterial cells
657 were incubated with Cd^{2+}-specific chelator, ECD. Figure 6 (ii) demonstrates that co-incubation
658 with ECD effectively reversed Cd^{2+}- induced loss of viability, restoring pink colour. This effect
659 was not observed in cells exposed to other metal ions, where ECD could not block metal induced
660 inhibition. Similarly, DMSA reversed the toxic effects of Hg^{2+} [Figure 6 (iii) and (iv)], while other
661 metal ions continued to attenuate cell viability. Notably, Since EDTA is a broad-spectrum metal
662 chelator, it restored viability across all metal-treated samples [Figure 6 (v) and (vi)]. Collectively,
663 these findings validate the high-throughput and multiplexing capability of the developed biosensor
664 platform, underscoring its potential for simultaneous detection of multiple toxic metal ions with
665 high specificity and sensitivity.

666

667

668

669

670

671

672

673

674

675

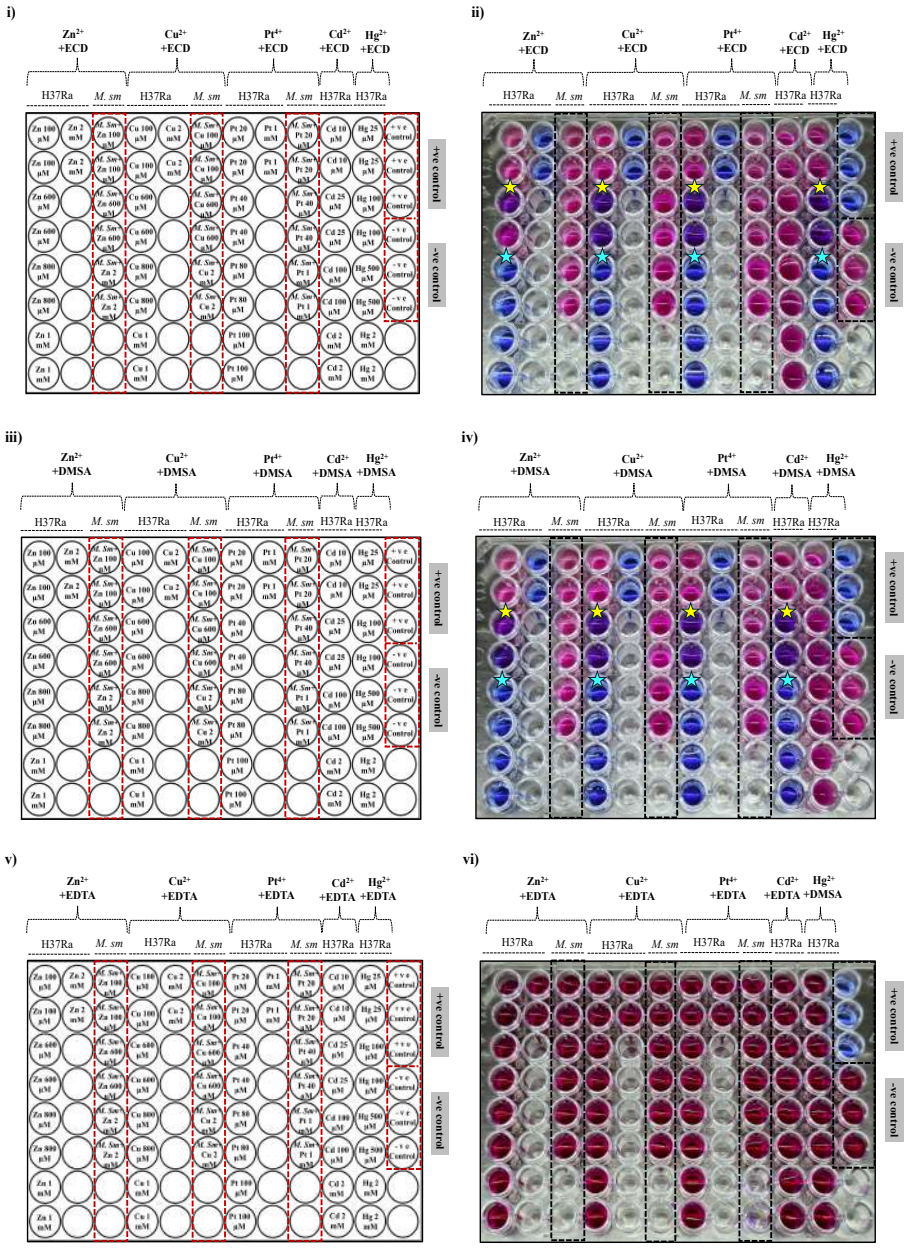
i)
ii)
iii)
iv)
v)
vi)
Zn2+ +ECD
Cu2+ +ECD
Pt4+ +ECD
Cd2+ +ECD
Hg2+ +ECD
Zn2+ +DMSA
Cu2+ +DMSA
Pt4+ +DMSA
Cd2+ +DMSA
Hg2+ +DMSA
Zn2+ +EDTA
Cu2+ +EDTA
Pt4+ +EDTA
Cd2+ +EDTA
Hg2+ +EDTA
H37Ra
M. sm
+ve control
-ve control

693 **Figure 6. Determination of specificity of the *Mtb* H37Ra-based multiplexing biosensor**
694 **platform.** (i) Schematic representation of the multiplexing biosensor platform along with Cd^{2+}
695 specific metal chelator (ECD) (ii) *Mtb* H37Ra cells (10^8 CFU/ml) were incubated with different
696 concentration of $ZnCl_2$,$CuCl_2$, $PtCl_4$, $CdCl_2$ and $HgCl_2$, along with ECD (1:1 ratio). ECD reversed
697 the inhibitory effect of Cd^{2+} rendering viable pink cells, whereas the effects of other metal ions
698 persisted (iii) Schematic representation of the multiplexing biosensor platform along with Hg^{2+}
699 specific metal chelator (DMSA). (iv) *Mtb* H37Ra cells (10^8 CFU/ml) were incubated with different
700 concentration of $ZnCl_2$,$CuCl_2$, $PtCl_4$, $CdCl_2$ and $HgCl_2$, along with DMSA in the ratio 1:1. DMSA
701 inhibited the effect of Hg^{2+} inducing viable pink cells, whereas the effect of other metal ions
702 persisted. (v) Schematic representation of plate-based biosensor platform in presence of common
703 metal chelator EDTA. (vi) *Mtb* H37Ra cells (10^8 CFU/ml) were allowed to grow in presence of
704 $ZnCl_2$,$CuCl_2$, $PtCl_4$, $CdCl_2$ and $HgCl_2$ along with EDTA in the ratio 1:1. The inhibitory effects of
705 test metal ions on mycobacterial cells were reversed by EDTA. For a baseline correction, H37Ra
706 cells were grown in the absence of toxic metal ions, as the live cell control. SufB intein-less
707 organism *Mycobacterium smegmatis (M. sm)* was used as additional experimental control and
708 treated under similar conditions. *M. sm* cells exhibited pink colour across a varied range of toxic
709 metal ions, suggesting their cell viability as an intein-independent phenomenon. The experiments
710 were performed in triplicates to confirm the reproducibility of data. Cyan stars- complete loss of
711 viability (blue) & Yellow stars- partial loss of viable cells (purple). ECD: Edetate Calcium
712 disodium, DMSA: Meso-2,3-Dimercaptosuccinic acid, EDTA: Ethylenediaminetetraacetic Acid.

713

714 In toto, the designed biosensor has demonstrated the potential of whole-cell *Mtb* H37Ra as an
715 indicator to detect toxic metal ions as well as TMEs in test samples. The specificity of the designed
716 metal-sensor was shown by the reversal of the inhibitory effects in the presence of Cd^{2+}- and Hg^{2+}-
717 specific metal chelators, ECD and DMSA, respectively. Detection of metal ions at a concentration
718 of 25 μM (Cd^{2+}) highlights the sensitivity of the biosensor platform, although it requires further
719 optimization to cover the lower concentration range of various metal ions. We propose the use of
720 whole-cell microorganisms carrying metal-sensing intein-bearing proteins as an indicator for the
721 presence of toxic metal ions in environmental samples. This is a user-friendly method that can be
722 performed in a 96-well microtiter plate, which would provide a colour change between blue and
723 pink while sensing metal ions. Since the activity of metal-sensing intein-carrying protein

724 sequences are unique for the indicator (whole-cell) organisms, in the unlikely event of
725 contamination in a biological facility, it should not raise concern about the validity of the results.

726 **Conclusion**

727 Heavy metal ions are persistent environmental contaminants that pose significant risks to both
728 ecological systems and human health. With the rising burden of metal pollution across diverse
729 environmental and biological matrices, there is a pressing need for sensitive, specific, and user-
730 friendly biosensing technology. Intein-mediated biosensors are emerging as promising tools in this
731 context, particularly due to their unique splicing mechanism that operates efficiently under
732 physiological conditions, eliminating the need for external cofactors or energy sources.[31,132] In this
733 study, *Mtb* H37Ra -based *in vitro* biosensor platform was developed, employing intein splicing
734 inhibition as a readout mechanism for the detection of toxic heavy metal ions (e.g., Cd^{2+} and Hg^{2+})
735 and other trace metal elements (Figure 7). The resulting alteration in mycobacterial viability is
736 captured through a rapid and quantifiable resazurin-based colorimetric assay that reports colour
737 change between blue-purple-pink. Importantly, the platform is adaptable for multiplex detection
738 of metal ions, including Zn^{2+}, Pt^{4+}, Cu^{2+}, Cd^{2+}, and Hg^{2+}, thereby offering a high-throughput
739 solution for complex sample screening (Figures 5 and 6). Further, this can be extended to sense
740 metal ions by other whole-cell microorganisms, harbouring unique metal-sensing intein-
741 containing proteins, hence offering a qualitative as well as quantitative detection method.

742 SufB is a critical component of SUF system, the exclusive pathway for Fe-S cluster assembly in
743 mycobacteria. Previous studies have also highlighted the pivotal role of *Mtb* SufB protein in Fe-
744 S cluster biogenesis, and mycobacterial survival.[54,133] Since the functionality of SUF protein
745 complex is dependent on generation of active SufB protein via splicing, splicing inhibition

746 presents a promising approach for antimicrobial intervention by targeting mycobacterial viability.
747 Several studies have shown that divalent cations ($Zn^{2+}$and Cu^{2+}), ROS, RNS, chlorine derivatives,
748 small molecules (cisplatin and diethanolamine) and zinc oxide nanoparticles can act as potent
749 splicing inhibitors. These agents have influenced mycobacterial survival, further validating the
750 relevance of targeting intein splicing for antimycobacterial drug development.[37,38,46,48,57,59,113–116]
751 Earlier work from our group has demonstrated that metal ions such as Cu^{2+}, Zn^{2+}, and Pt^{4+} inhibit
752 SufB splicing, establishing a correlation between metal-induced stress and altered intein splicing
753 activity in *Mtb*.[38] Building on these findings, the current work explores regulatory roles of toxic
754 metal ions on *Mtb* SufB splicing and cleavage activity. Alamar blue assay was employed to
755 examine the influence of TMEs and toxic metal ions on the viability of *Mtb* cells. The outcome of
756 this research will advance the real time application of H37Ra based whole-cell biosensor to detect
757 wide range of metal ions. The platform described herein is robust, enabling multiplex screening of
758 metal ions while maintaining specificity and sensitivity. Importantly, cellular viability loss in
759 response to metal exposure is linked to an observable colour shift between blue and pink, providing
760 a quantifiable readout for metal ion detection in test samples.

761 In this study, splicing inhibition was evaluated both *in vitro*, using purified SufB protein and *in*
762 *vivo* within H37Ra cells in a whole-cell biosensor platform, where the observed effects on
763 mycobacterial viability were correlated to SufB splicing inhibition. Given that H37Ra is a slow-
764 growing strain with a mean generation time of approximately 44 hours, the experimental window
765 was established at four days to encompass at least two full generations, permitting effective
766 assessment of metal-induced viability changes.[134–136] Notably, the logarithmic growth phase of
767 mycobacteria extends from four to twenty days, ensuring that the platform remains adaptable to
768 varied experimental requirements. To further strengthen our hypothesis, SufB intein less organism,

769 *M. sm* control was included; viability of *M. sm* persisted throughout the experimental period,
770 suggesting that the tested metal ions do not elicit growth inhibitory or toxic effects in the absence
771 of SufB intein. *Mtb* contains three intein containing proteins; SufB, RecA and DnaB. While SufB
772 is essential for Fe-S cluster assembly, RecA and DnaB play pivotal roles during DNA replication;
773 taken together these proteins are critical for mycobacterial survival.[137–139] Although current study
774 explains loss of mycobacterial cell viability as a result of inhibition of *Mtb* SufB splicing, the
775 possibility of RecA and DnaB splicing inhibition by the test metal ions cannot be ruled completely.
776 Currently, there are no literatures to show inhibitory effect of metal ions other than Zn^{2+} on *Mtb*
777 DnaB splicing.[44] Moreover there are alternative helicases present in mycobacteria to take over the
778 function of DnaB.[120–122] Several studies have reported regulatory roles of Zn^{2+}, Cd^{2+}, Co^{2+}, Ni^{2+},
779 Cu^{+}/Cu^{2+}, CisPt ions on *Mtb* RecA intein splicing.[40,42,48,113] However, current study has not
780 evaluated the RecA intein inhibition in mycobacteria. Hence, this approach offers a multiplexing
781 biosensor unit which can accommodate cell viability detection via splicing inhibition in many
782 organisms carrying different metal-sensitive intein containing proteins simultaneously.

783 The use of non-genetically modified *Mtb* H37Ra cells ensures biosecurity compliance while
784 providing a biologically relevant sensing chassis. These mycobacterial cells are not only easy to
785 cultivate and maintain but also exhibit remarkable long-term viability, supporting extended shelf-
786 life and storage without specialized conditions. The platform also demonstrates good sensitivity in
787 detecting metal ions over a broad dynamic range, and substrate specificity, making it suitable for
788 metal ion screening in standard laboratory setups.

789 However, some limitations persist such as complex environmental or biological samples
790 containing mixtures of multiple metal ions may result in signal overlap or cross-reactivity with
791 variable binding affinities. Furthermore, while microbial whole-cell biosensors offer an excellent

792 alternative for initial screening and field deployment, advanced physicochemical instruments
793 remain crucial when trace-level quantification is required, where intein activity may not be
794 efficiently regulated.

795 In summary, our findings highlight the potential of whole cell intein-based biosensors as user-
796 friendly, and cost-effective tools for the detection of toxic metal and trace metal ions. Future work
797 should aim to refine their activity, enhancing environmental robustness, and advancing the
798 platform from lab-scale to deployable technologies. This can be accelerated through collaborative
799 efforts across academic, industrial, and governmental sectors.

800

801
802
803
804
805
806
807
808

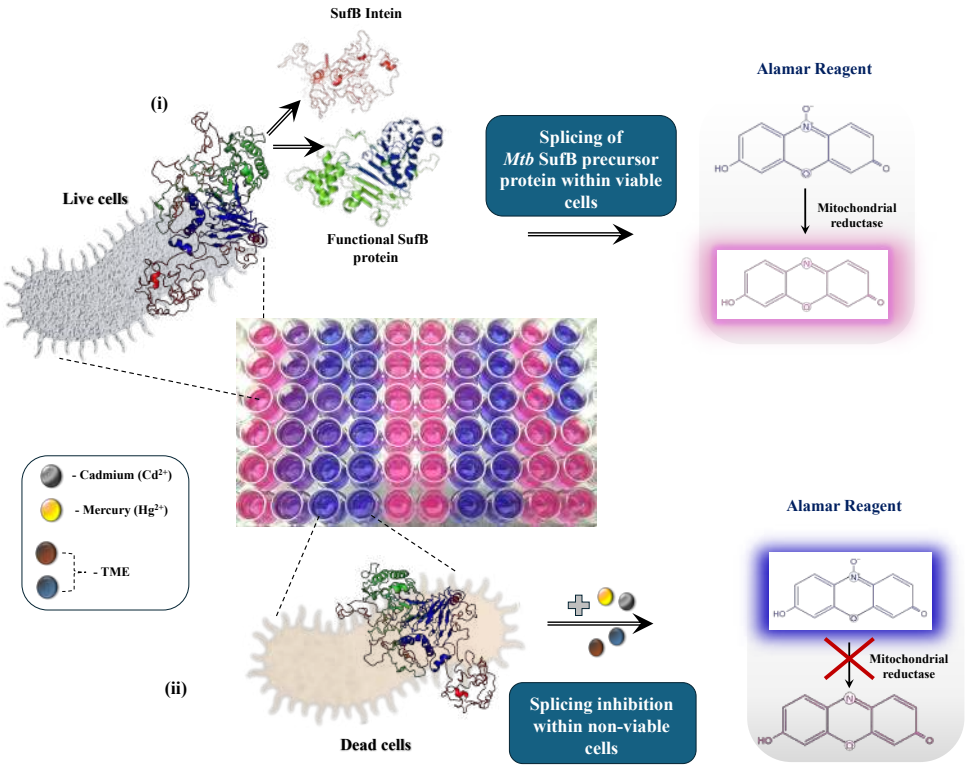

809

810 **Figure 7. Schematic representation explaining the principle of *Mtb* H37Ra-based**
811 **multiplexing biosensor platform.** Whole-cell mycobacteria (H37Ra) were used as biological

indicator for the detection of toxic metal ions (Cd^{2+} and Hg^{2+}) and other trace metal elements (TME). (i) Intein splicing under normal physiological conditions generates functional SufB protein, while viable mycobacterial cells convert resazurin (blue) to resorufin (pink). (ii) In the presence of toxic metal ions Cd^{2+} and Hg^{2+} and TME, SufB intein splicing is inhibited resulting in non-viable mycobacterial cells, thus there is no conversion of resazurin (blue) to resorufin (pink).

Acknowledgments

The plasmids used in this study are borrowed from Prof. Marlene Belfort's Lab, SUNY, Albany, NY, USA. Our sincere gratitude to the Central Instrumentation Facility (CIF) at OUAT (Odisha University of Agriculture & Technology), Bhubaneswar, and Dr. S.K. Dash for his help in conducting the ICP-OES analysis at OUAT, Bhubaneswar.

Funding

Ms. Ashwaria Mehra is supported by INSPIRE fellowship (DST/INSPIRE/03/2021/002800/IF 190921); INSPIRE Division, DST, Government of India. This work was also supported by the UGC-DAE consortium for scientific research (UGC-DAE-CSR-KC/CRS/15/IOP/08/0562), Kolkata, India.

Author Contributions

AM: Writing – Original Draft, Writing - Review & Editing, Methodology, Investigation, Formal analysis, Data curation, Visualization, Validation, Software, Resources, Funding acquisition; **AN:** Conceptualization, Methodology, Investigation, Formal analysis, Data curation; Writing - Review & Editing, ; **SN:** Conceptualization, Writing - Original Draft, Writing - Review & Editing, Project administration, Supervision, Methodology, Investigation, Resources, Funding acquisition.

835 **Declaration of competing interest**

836 The authors declare that they have no known competing financial interests or personal
837 relationships that could have appeared to influence the work reported in this paper.

838 **Data availability**

839 Data will be made available on request.

840 **Abbreviations:**

841 Ni-NTA: Nickel-nitrilotriacetic acid
842 TCEP.HCl: Tris 2-carboxyl ethyl phosphine. Hydrochloric acid

843 IPTG: Isopropyl β-d-1-thiogalactopyranoside

844 Trp: Tryptophan

845 SDS: Sodium Dodecyl Sulfate

846 PAGE: Polyacrylamide gel electrophoresis

847 ICP-OES: Inductively Coupled Plasma Optical Emission Spectroscopy

848 UV-Vis: UV-visible spectroscopy

849 PVDF: Polyvinylidene fluoride

850 BSA: Bovine serum albumin

851 *Mtb*: *Mycobacterium tuberculosis*

852 WT: Wild type

853 SI: Splicing inactive

854 Cd^{2+}: Cadmium

855 Hg^{2+}: Mercury

856 Pb^{2+}: Lead

857 Cr^{3+}: Chromium

858 **References**

859 (1) Velusamy, K.; Periyasamy, S.; Kumar, P. S.; Rangasamy, G.; Nisha Pauline, J. M.;
860 Ramaraju, P.; Mohanasundaram, S.; Nguyen Vo, D. V. Biosensor for Heavy Metals
861 Detection in Wastewater: A Review. *Food and Chemical Toxicology* **2022**, *168*, 113307.
862 https://doi.org/10.1016/J.FCT.2022.113307.

863 (2) Duffus, J. H. *"heavy Metals" - A Meaningless Term? (IUPAC Technical Report)*; Walter
864 de Gruyter GmbH, 2002; Vol. 74.
865 https://www.degruyterbrill.com/document/doi/10.1351/pac200274050793/html (accessed
866 2025-06-16).

867 (3) Turdean, G. L.; Ozkan, S. A. Design and Development of Biosensors for the Detection of
868 Heavy Metal Toxicity. *International Journal of Electrochemistry* **2011**, *2011* (1), 343125.
869 https://doi.org/10.4061/2011/343125.

870 (4) Singh, R.; Gautam, N.; Mishra, A.; Gupta, R. Heavy Metals and Living Systems: An
871 Overview. *Indian J Pharmacol* **2011**, *43* (3), 246–253. https://doi.org/10.4103/0253-
872 7613.81505.

873 (5) Angon, P. B.; Islam, M. S.; KC, S.; Das, A.; Anjum, N.; Poudel, A.; Suchi, S. A. Sources,
874 Effects and Present Perspectives of Heavy Metals Contamination: Soil, Plants and Human
875 Food Chain. *Heliyon* **2024**, *10* (7), e28357.
876 https://doi.org/10.1016/J.HELIYON.2024.E28357.

877 (6) Alengebawy, A.; Abdelkhalek, S. T.; Qureshi, S. R.; Wang, M. Q. Heavy Metals and
878 Pesticides Toxicity in Agricultural Soil and Plants: Ecological Risks and Human Health
879 Implications. *Toxics* **2021**, *9* (3), 42. https://doi.org/10.3390/TOXICS9030042.

880 (7) Jaishankar, M.; Tseten, T.; Anbalagan, N.; Mathew, B. B.; Beeregowda, K. N. Toxicity,
881 Mechanism and Health Effects of Some Heavy Metals. *Interdiscip Toxicol* **2014**, *7* (2),
882 60–72. https://doi.org/10.2478/INTOX-2014-0009.

883 (8) Hassani, S.; Rezaei Akmal, M.; Salek Maghsoudi, A.; Rahmani, S.; Vakhshiteh, F.;
884 Norouzi, P.; Ganjali, M. R.; Abdollahi, M. High-Performance Voltammetric Aptasensing
885 Platform for Ultrasensitive Detection of Bisphenol A as an Environmental Pollutant. *Front*
886 *Bioeng Biotechnol* **2020**, *8*, 574846. https://doi.org/10.3389/FBIOE.2020.574846.

887 (9) Odobašić, A.; Šestan, I.; Begić, S.; Odobašić, A.; Šestan, I.; Begić, S. *Biosensors for*
888 *Determination of Heavy Metals in Waters*; IntechOpen, 2019.
889 https://doi.org/10.5772/INTECHOPEN.84139.

890 (10) Ramnani, P.; Saucedo, N. M.; Mulchandani, A. Carbon Nanomaterial-Based
891 Electrochemical Biosensors for Label-Free Sensing of Environmental Pollutants.
892 *Chemosphere* **2016**, *143*, 85–98. https://doi.org/10.1016/J.CHEMOSPHERE.2015.04.063.

893 (11) Pena-Pereira, F.; Wojnowski, W.; Tobiszewski, M. AGREE - Analytical GREEnness
894 Metric Approach and Software. *Anal Chem* **2020**, *92* (14), 10076–10082.
895 https://doi.org/10.1021/acs.analchem.0c01887.

896 (12) Pearson, J. E.; Gill, A.; Vadgama, P. Analytical Aspects of Biosensors. *Ann Clin Biochem*
897 **2000**, *37* (2), 119–145. https://doi.org/10.1258/0004563001899131.

898 (13) Malandain, C.; Fayolle, F.; Bedouelle, H. Biosensors for the Environment. *Oil & Gas*
899 *Science and Technology* **2005**, *60* (6), 887–897. https://doi.org/10.2516/OGST:2005062.

900 (14) Bontidean, I.; Berggren, C.; Johansson, G.; Csöregi, E.; Mattiasson, B.; Lloyd, J. R.;
901 Jakeman, K. J.; Brown, N. L. Detection of Heavy Metal Ions at Femtomolar Levels Using
902 Protein-Based Biosensors. *Anal Chem* **1998**, *70* (19), 4162–4169.
903 https://doi.org/10.1021/ac9803636.

904 (15) Blake, D. A.; Jones, R. M.; Blake, R. C.; Pavlov, A. R.; Darwish, I. A.; Yu, H. Antibody-
905 Based Sensors for Heavy Metal Ions. *Biosens Bioelectron* **2001**, *16* (9–12), 799–809.
906 https://doi.org/10.1016/S0956-5663(01)00223-8.

907 (16) Chouteau, C.; Dzyadevych, S.; Durrieu, C.; Chovelon, J. M. A Bi-Enzymatic Whole Cell
908 Conductometric Biosensor for Heavy Metal Ions and Pesticides Detection in Water
909 Samples. *Biosens Bioelectron* **2005**, *21* (2), 273–281.
910 https://doi.org/10.1016/J.BIOS.2004.09.032.

911 (17) Mohammadi, Z. B.; Zhang, F.; Kharazmi, M. S.; Jafari, S. M. Nano-Biocatalysts for Food
912 Applications; Immobilized Enzymes within Different Nanostructures. *Crit Rev Food Sci*
913 *Nutr* **2023**, *63* (32), 11351–11369. https://doi.org/10.1080/10408398.2022.2092719.

914 (18) Sun, G.; Wei, X.; Zhang, D.; Huang, L.; Liu, H.; Fang, H. Immobilization of Enzyme
915 Electrochemical Biosensors and Their Application to Food Bioprocess Monitoring.
916 *Biosensors (Basel)* **2023**, *13* (9), 886. https://doi.org/10.3390/BIOS13090886.

917 (19) Kakkar, P.; Jaffery, F. N. Biological Markers for Metal Toxicity. *Environ Toxicol*
918 *Pharmacol* **2005**, *19* (2), 335–349. https://doi.org/10.1016/J.ETAP.2004.09.003.

919 (20) Castillo, J.; Gáspár, S.; Leth, S.; Niculescu, M.; Mortari, A.; Bontidean, I.; Soukharev, V.;
920 Dorneanu, S. A.; Ryabov, A. D.; Csöregi, E. Biosensors for Life Quality: Design,
921 Development and Applications. *Sens Actuators B Chem* **2004**, *102* (2), 179–194.
922 https://doi.org/10.1016/J.SNB.2004.04.084.

(21) Bousse, L. Whole Cell Biosensors. *Sens Actuators B Chem* **1996**, *34* (1–3), 270–275. https://doi.org/10.1016/S0925-4005(96)01906-5.

(22) Stenger, D. A.; Gross, G. W.; Keefer, E. W.; Shaffer, K. M.; Andreadis, J. D.; Ma, W.; Pancrazio, J. J. Detection of Physiologically Active Compounds Using Cell-Based Biosensors. *Trends Biotechnol* **2001**, *19* (8), 304–309. https://doi.org/10.1016/S0167-7799(01)01690-0.

(23) Wang, Y.-Z.; Christopher, J. K.; Yong, Y.-C.; Zhai, D.-D. *Nutrient Detection with Whole-Cell Biosensors*; Springer, Cham, 2019. https://doi.org/10.1007/978-3-319-47405-2_110-1.

(24) Mihaela, G.; Mihaela, G. A Short Review on Cell-Based Biosensing: Challenges and Breakthroughs in Biomedical Analysis. *J Biomed Res* **2021**, *35* (4), 255–263. https://doi.org/10.7555/JBR.34.20200128.

(25) Raut, N.; O'Connor, G.; Pasini, P.; Daunert, S. Engineered Cells as Biosensing Systems in Biomedical Analysis. *Anal Bioanal Chem* **2012**, *402* (10), 3147–3159. https://doi.org/10.1007/s00216-012-5756-6.

(26) Gui, Q.; Lawson, T.; Shan, S.; Yan, L.; Liu, Y. The Application of Whole Cell-Based Biosensors for Use in Environmental Analysis and in Medical Diagnostics. *Sensors* **2017**, *17* (7), 1623. https://doi.org/10.3390/S17071623.

(27) Kang, C.; Shrestha, K. L.; Kwon, S.; Park, S.; Kim, J.; Kwon, Y. Intein-Mediated Protein Engineering for Cell-Based Biosensors. *Biosensors (Basel)* **2022**, *12* (5), 283. https://doi.org/10.3390/BIOS12050283.

(28) Jeon, H.; Lee, E.; Kim, D.; Lee, M.; Ryu, J.; Kang, C.; Kim, S.; Kwon, Y. Cell-Based Biosensors Based on Intein-Mediated Protein Engineering for Detection of Biologically Active Signaling Molecules. *Anal Chem* **2018**, *90* (16), 9779–9786. https://doi.org/10.1021/acs.analchem.8b01481.

(29) Lee, E.; Shrestha, K. L.; Kang, S.; Ramakrishnan, N.; Kwon, Y. Cell-Based Sensors for the Detection of EGF and EGF-Stimulated Ca2+ Signaling. *Biosensors (Basel)* **2023**, *13* (3), 383. https://doi.org/10.3390/BIOS13030383/S1.

(30) Jeon, H.; Lee, M.; Jang, W.; Kwon, Y. Intein-Mediated Protein Engineering for Biosensor Fabrication. *Biochip J* **2016**, *10* (4), 277–287. https://doi.org/10.1007/S13206-016-0404-4.

(31) Mills, K. V.; Johnson, M. A.; Perler, F. B. Protein Splicing: How Inteins Escape from Precursor Proteins. *Journal of Biological Chemistry* **2014**, *289* (21), 14498–14505. https://doi.org/10.1074/JBC.R113.540310.

(32) Perler, F. B. Protein Splicing Mechanisms and Applications. *IUBMB Life* **2005**, *57* (7), 469–476. https://doi.org/10.1080/15216540500163343.

(33) Panda, S.; Nanda, A.; Nasker, S. S.; Sen, D.; Mehra, A.; Nayak, S. Metal Effect on Intein Splicing: A Review. *Biochimie* **2021**, *185*, 53–67. https://doi.org/10.1016/J.BIOCHI.2021.03.006.

(34) Nichols, N. M.; Benner, J. S.; Martin, D. D.; Evans, T. C. Zinc Ion Effects on Individual Ssp DNaE Intein Splicing Steps: Regulating Pathway Progression. *Biochemistry* **2003**, *42* (18), 5301–5311. https://doi.org/https://doi.org/10.1021/bi020679e.

(35) Chan, H.; Pearson, C. S.; Green, C. M.; Li, Z.; Zhang, J.; Belfort, G.; Shekhtman, A.; Li, H.; Belfort, M. Exploring Intein Inhibition by Platinum Compounds as an Antimicrobial Strategy. *Journal of Biological Chemistry* **2016**, *291* (43), 22661–22670. https://doi.org/10.1074/JBC.M116.747824.

(36) Green, C. M.; Li, Z.; Smith, A. D.; Novikova, O.; Bacot-Davis, V. R.; Gao, F.; Hu, S.; Banavali, N. K.; Thiele, D. J.; Li, H.; Belfort, M. Spliceosomal Prp8 Intein at the Crossroads of Protein and RNA Splicing. *PLoS Biol* **2019**, *17* (10), e3000104. https://doi.org/10.1371/JOURNAL.PBIO.3000104.

(37) Ojha, D. K.; Mehra, A.; Rout, S. S.; Giri, S.; Nayak, S. Bactericidal Activity of ZnO Nanoparticles–Anti-TB Drug Combination towards the H37Rv Strain and Multidrug-Resistant Isolates of Mycobacterium Tuberculosis via SufB Splicing Inhibition. *Mater Adv* **2025**, *6* (15), 5242–5259. https://doi.org/10.1039/D4MA01224K.

(38) Panda, S.; Nanda, A.; Nasker, S. S.; Mehra, A.; Ojha, D. K.; Mohanty, P. S.; Nayak, S. Metal Regulation of Mycobacterium Tuberculosis SufB Intein Splicing at the Host–Pathogen Crossroad. *Clin Sci* **2023**, *137* (14), 1027–1048. https://doi.org/10.1042/CS20230307.

(39) Poland, B. W.; Xu, M. Q.; Quiocho, F. A. Structural Insights into the Protein Splicing Mechanism of PI-SceI. *Journal of Biological Chemistry* **2000**, *275* (22), 16408–16413. https://doi.org/10.1074/JBC.275.22.16408.

(40) Mills, K. V.; Paulus, H. Reversible Inhibition of Protein Splicing by Zinc Ion. *Journal of Biological Chemistry* **2001**, *276* (14), 10832–10838. https://doi.org/10.1074/JBC.M011149200.

(41) Van Roey, P.; Pereira, B.; Li, Z.; Hiraga, K.; Belfort, M.; Derbyshire, V. Crystallographic and Mutational Studies of Mycobacterium Tuberculosis RecA Mini-Inteins Suggest a Pivotal Role for a Highly Conserved Aspartate Residue. *J Mol Biol* **2007**, *367* (1), 162–173. https://doi.org/10.1016/J.JMB.2006.12.050.

990 (42) Zhang, L.; Zheng, Y.; Xi, Z.; Luo, Z.; Xu, X.; Wang, C.; Liu, Y. Metal Ions Binding to
991 RecA Inteins from Mycobacterium Tuberculosis. *Mol Biosyst* **2009**, *5* (6), 644–650.
992 https://doi.org/10.1039/B903144H.

993 (43) Sun, P.; Ye, S.; Ferrandon, S.; Evans, T. C.; Xu, M. Q.; Rao, Z. Crystal Structures of an
994 Intein from the Split DnaE Gene of Synechocystis Sp. PCC6803 Reveal the Catalytic
995 Model Without the Penultimate Histidine and the Mechanism of Zinc Ion Inhibition of
996 Protein Splicing. *J Mol Biol* **2005**, *353* (5), 1093–1105.
997 https://doi.org/10.1016/J.JMB.2005.09.039.

998 (44) Woods, D.; Vangaveti, S.; Egbanum, I.; Sweeney, A. M.; Li, Z.; Bacot-Davis, V.;
999 Lesassier, D. S.; Stanger, M.; Hardison, G. E.; Li, H.; Belfort, M.; Lennon, C. W.
1000 Conditional DnaB Protein Splicing Is Reversibly Inhibited by Zinc in Mycobacteria. *mBio*
1001 **2020**, *11* (4), 1–14. https://doi.org/10.1128/mBio.01403-20.

1002 (45) Pearson, C. S.; Belfort, G.; Belfort, M.; Shekhtman, A. Backbone Assignments of Mini-
1003 RecA Intein with Short Native Exteins and an Active N-Terminal Catalytic Cysteine.
1004 *Biomol NMR Assign* **2015**, *9* (2), 235–238. https://doi.org/10.1007/s12104-014-9581-z.

1005 (46) Li, Z.; Fu, B.; Green, C. M.; Liu, B.; Zhang, J.; Lang, Y.; Chaturvedi, S.; Belfort, M.;
1006 Liao, G.; Li, H. Cisplatin Protects Mice from Challenge of Cryptococcus Neoformans by
1007 Targeting the Prp8 Intein. *Emerg Microbes Infect* **2019**, *8* (1), 895–908.
1008 https://doi.org/10.1080/22221751.2019.1625727.

1009 (47) Zhang, L.; Xiao, N.; Pan, Y.; Zheng, Y.; Pan, Z.; Luo, Z.; Xu, X.; Liu, Y. Binding and
1010 Inhibition of Copper Ions to RecA Inteins from Mycobacterium Tuberculosis. *Chemistry -*
1011 *A European Journal* **2010**, *16* (14), 4297–4306.
1012 https://doi.org/https://doi.org/10.1002/chem.200903584.

1013 (48) Zhang, L.; Zheng, Y.; Callahan, B.; Belfort, M.; Liu, Y. Cisplatin Inhibits Protein
1014 Splicing, Suggesting Inteins as Therapeutic Targets in Mycobacteria. *Journal of*
1015 *Biological Chemistry* **2011**, *286* (2), 1277–1282.
1016 https://doi.org/10.1074/JBC.M110.171124.

1017 (49) Dassa, B.; Amitai, G.; Caspi, J.; Schueler-Furman, O.; Pietrokovski, S. Trans Protein
1018 Splicing of Cyanobacterial Split Inteins in Endogenous and Exogenous Combinations.
1019 *Biochemistry* **2007**, *46* (1), 322–330. https://doi.org/10.1021/bi0611762.

1020 (50) Gramespacher, J. A.; Stevens, A. J.; Nguyen, D. P.; Chin, J. W.; Muir, T. W. Intein
1021 Zymogens: Conditional Assembly and Splicing of Split Inteins via Targeted Proteolysis. *J*
1022 *Am Chem Soc* **2017**, *139* (24), 8074–8077. https://doi.org/10.1021/JACS.7B02618.

1023 (51) Skretas, G.; Wood, D. W. Regulation of Protein Activity with Small-Molecule-Controlled
1024 Inteins. *Protein Science* **2005**, *14* (2), 523–532. https://doi.org/10.1110/PS.04996905.

1025 (52) Ozawa, T.; Nogami, S.; Sato, M.; Ohya, Y.; Umezawa, Y. A Fluorescent Indicator for
1026 Detecting Protein−Protein Interactions in Vivo Based on Protein Splicing. *Anal Chem*
1027 **2000**, *72* (21), 5151–5157. https://doi.org/10.1021/AC000617Z.

1028 (53) Huet, G.; Daffé, M.; Saves, I. Identification of the Mycobacterium Tuberculosis SUF
1029 Machinery as the Exclusive Mycobacterial System of [Fe-S] Cluster Assembly: Evidence
1030 for Its Implication in the Pathogen's Survival. *J Bacteriol* **2005**, *187* (17), 6137–6146.
1031 https://doi.org/10.1128/jb.187.17.6137-6146.2005.

1032 (54) Huet, G.; Castaing, J. P.; Fournier, D.; Daffé, M.; Saves, I. Protein Splicing of SufB Is
1033 Crucial for the Functionality of the Mycobacterium Tuberculosis SUF Machinery. *J*
1034 *Bacteriol* **2006**, *188* (9), 3412–3414. https://doi.org/10.1128/JB.188.9.3412-3414.2006.

1035 (55) Panda, S.; Nanda, A.; Sahu, N.; Ojha, D. K.; Pradhan, B.; Rai, A.; Suryawanshi, A. R.;
1036 Banavali, N.; Nayak, S. SufB Intein Splicing in Mycobacterium Tuberculosis Is
1037 Influenced by Two Remote Conserved N-Extein Histidines. *Biosci Rep* **2022**, *42* (3),
1038 20212207. https://doi.org/10.1042/BSR20212207/230724.

1039 (56) Friedel, K.; Popp, M. A.; Matern, J. C. J.; Gazdag, E. M.; Thiel, I. V.; Volkmann, G.;
1040 Blankenfeldt, W.; Mootz, H. D. A Functional Interplay between Intein and Extein
1041 Sequences in Protein Splicing Compensates for the Essential Block B Histidine. *Chem Sci*
1042 **2018**, *10* (1), 239–251. https://doi.org/10.1039/C8SC01074A.

1043 (57) Kelley, D. S.; Lennon, C. W.; Li, Z.; Miller, M. R.; Banavali, N. K.; Li, H.; Belfort, M.
1044 Mycobacterial DnaB Helicase Intein as Oxidative Stress Sensor. *Nat Commun* **2018**, *9* (1),
1045 1–15. https://doi.org/10.1038/S41467-018-06554-X.

1046 (58) Mills, K. V.; Lew, B. M.; Jiang, S. Q.; Paulus, H. Protein Splicing in Trans by Purified N-
1047 and C-Terminal Fragments of the Mycobacterium Tuberculosis RecA Intein. *Proc Natl*
1048 *Acad Sci U S A* **1998**, *95* (7), 3543–3548. https://doi.org/10.1073/pnas.95.7.3543.

1049 (59) Gangopadhyay, J. P.; Jiang, S. qin; Paulus, H. An in Vitro Screening System for Protein
1050 Splicing Inhibitors Based on Green Fluorescent Protein as an Indicator. *Anal Chem* **2003**,
1051 *75* (10), 2456–2462. https://doi.org/10.1021/ac020756b.

1052 (60) Nanda, A.; Nasker, S. S.; Kushwaha, A. K.; Ojha, D. K.; Dearden, A. K.; Nayak, S. K.;
1053 Nayak, S. Gold Nanoparticles Augment N-Terminal Cleavage and Splicing Reactions in
1054 Mycobacterium Tuberculosis SufB. *Front Bioeng Biotechnol* **2021**, *9*, 773303.
1055 https://doi.org/10.3389/FBIOE.2021.773303.

1056 (61) Chemiluminescence, B.; Li, J.; Xing, H.; Wang, E.; Zhao, J.; Li, D.; Ma, J.; Suhartono, E.;
1057 Thalib, I.; Aflanie, I.; Noor, Z.; Idroes, R. Study of Interaction between Cadmium and
1058 Bovine Serum Albumin with UV-Vis Spectrocopy Approach. In *IOP Conference Series:*

1059 *Materials Science and Engineering*; IOP Publishing, 2018; Vol. 350, p 012008.
1060 https://doi.org/10.1088/1757-899X/350/1/012008.

1061 (62) Grzyska, P. K.; Hausinger, R. P.; Proshlyakov, D. A. Metal and Substrate Binding to an
1062 Fe(II) Dioxygenase Resolved by UV Spectroscopy with Global Regression Analysis. *Anal*
1063 *Biochem* **2010**, *399* (1), 64–71. https://doi.org/10.1016/J.AB.2009.11.022.

1064 (63) Plotnikova, O. A.; Mel'nikov, A. G.; Mel'nikov, G. V.; Gubina, T. I. Quenching of
1065 Tryptophan Fluorescence of Bovine Serum Albumin under the Effect of Ions of Heavy
1066 Metals. *Opt Spectrosc* **2016**, *120* (1), 65–69.
1067 https://doi.org/https://doi.org/10.1134/S0030400X16010148.

1068 (64) Oliveira, A.; Baccana, N.; Cadore, S. Evaluation of Metal Ions in Rice Samples:
1069 Extraction and Direct Determination by ICP OES. *J Braz Chem Soc* **2012**, *23* (5), 838–
1070 845. https://doi.org/10.1590/S0103-50532012000500008.

1071 (65) Harrington, J. M.; Young, D. J.; Essader, A. S.; Sumner, S. J.; Levine, K. E. Analysis of
1072 Human Serum and Whole Blood for Mineral Content by ICP-MS and ICP-OES:
1073 Development of a Mineralomics Method. *Biol Trace Elem Res* **2014**, *160* (1), 132–142.
1074 https://doi.org/10.1007/s12011-014-0033-5.

1075 (66) Punjabi, K.; Mehta, S.; Chavan, R.; Chitalia, V.; Deogharkar, D.; Deshpande, S.
1076 Efficiency of Biosynthesized Silver and Zinc Nanoparticles against Multi-Drug Resistant
1077 Pathogens. *Front Microbiol* **2018**, *9* (SEP), 376058.
1078 https://doi.org/https://doi.org/10.3389/fmicb.2018.02207.

1079 (67) Longhin, E. M.; El Yamani, N.; Rundén-Pran, E.; Dusinska, M. The Alamar Blue Assay
1080 in the Context of Safety Testing of Nanomaterials. *Frontiers in Toxicology* **2022**, *4*,
1081 981701. https://doi.org/10.3389/FTOX.2022.981701.

1082 (68) Yang, L.; Zhang, Y.; Wang, F.; Luo, Z.; Guo, S.; Strähle, U. Toxicity of Mercury:
1083 Molecular Evidence. *Chemosphere* **2020**, *245*, 125586.
1084 https://doi.org/10.1016/J.CHEMOSPHERE.2019.125586.

1085 (69) Aljerf, L.; Almasri, N.; Access, O. Mercury Toxicity: Ecological Features of Organic
1086 Phase of Mercury in Biota-Part I. *Inorganic Chemical Sciences* **2018**, *3* (3).
1087 https://doi.org/10.32474/AOICS.2018.03.000157.

1088 (70) Budnik, L. T.; Casteleyn, L. Mercury Pollution in Modern Times and Its Socio-Medical
1089 Consequences. *Science of The Total Environment* **2019**, *654*, 720–734.
1090 https://doi.org/10.1016/J.SCITOTENV.2018.10.408.

1091 (71) Dash, H. R.; Mangwani, N.; Das, S. Characterization and Potential Application in
1092 Mercury Bioremediation of Highly Mercury-Resistant Marine Bacterium Bacillus

Thuringiensis PW-05. *Environmental Science and Pollution Research* **2014**, *21* (4), 2642–2653. https://doi.org/10.1007/s11356-013-2206-8.

(72) Tang, W.; Zhang, W.; Zhao, Y.; Zhang, H.; Shan, B. Basin-Scale Comprehensive Assessment of Cadmium Pollution, Risk, and Toxicity in Riverine Sediments of the Haihe Basin in North China. *Ecol Indic* **2017**, *81*, 295–301. https://doi.org/10.1016/J.ECOLIND.2017.06.011.

(73) White, P. J.; Brown, P. H. Plant Nutrition for Sustainable Development and Global Health. *Ann Bot* **2010**, *105* (7), 1073–1080. https://doi.org/10.1093/AOB/MCQ085.

(74) Losada Ros, M. T.; Al-Enezi, E.; Cesarini, E.; Canonico, B.; Bucci, C.; Martins, M. V. A.; Papa, S.; Frontalini, F. Assessing the Cadmium Effects on the Benthic Foraminifer Ammonia Cf. Parkinsoniana: An Acute Toxicity Test. *Water (Basel)* **2020**, *12* (4), 1018. https://doi.org/10.3390/W12041018.

(75) Dong, F.; Zhu, X.; Qian, W.; Wang, P.; Wang, J. Combined Effects of CO2-Driven Ocean Acidification and Cd Stress in the Marine Environment: Enhanced Tolerance of Phaeodactylum Tricornutum to Cd Exposure. *Mar Pollut Bull* **2020**, *150*, 110594. https://doi.org/10.1016/J.MARPOLBUL.2019.110594.

(76) Atamaleki, A.; Sadani, M.; Raoofi, A.; Miri, A.; Bajestani, S. G.; Fakhri, Y.; Heidarinejad, Z.; Mousavi Khaneghah, A. The Concentration of Potentially Toxic Elements (PTEs) in Eggs: A Global Systematic Review, Meta-Analysis and Probabilistic Health Risk Assessment. *Trends Food Sci Technol* **2020**, *95*, 1–9. https://doi.org/10.1016/J.TIFS.2019.11.003.

(77) Stankovic, S.; Kalaba, P.; Stankovic, A. R. Biota as Toxic Metal Indicators. *Environ Chem Lett* **2014**, *12* (1), 63–84. https://doi.org/10.1007/s10311-013-0430-6.

(78) Joe, M. H.; Lee, K. H.; Lim, S. Y.; Im, S. H.; Song, H. P.; Lee, I. S.; Kim, D. H. Pigment-Based Whole-Cell Biosensor System for Cadmium Detection Using Genetically Engineered Deinococcus Radiodurans. *Bioprocess Biosyst Eng* **2012**, *35* (1–2), 265–272. https://doi.org/10.1007/s00449-011-0610-3.

(79) Guertin, J.; Jacobs, J. A.; Avakian, C. P. *Chromium(VI) Handbook*, 1st ed.; CRC Press, 2004. https://doi.org/10.1201/9780203487969.

(80) Dawra, N.; Dabas, N. Advances in Spectrophotometric Determination of Chromium(III) and Chromium(VI) in Water: A Review. *Int J Environ Anal Chem* **2024**, *104* (13), 2994–3015. https://doi.org/10.1080/03067319.2022.2076224.

(81) Sheehan, P. J.; Meyer, D. M.; Sauer, M. M.; Paustenbach, D. J. Assessment of the Human Health Risks Posed by Exposure to Chromium-contaminated Soils. *Journal of Toxicology*

and Environmental Health, Part A Current Issues **1991**, *32* (2), 161–201. https://doi.org/10.1080/15287399109531476.

(82) Mishra, S.; Bharagava, R. N. Toxic and Genotoxic Effects of Hexavalent Chromium in Environment and Its Bioremediation Strategies. *Journal of Environmental Science and Health, Part C* **2016**, *34* (1), 1–32. https://doi.org/10.1080/10590501.2015.1096883.

(83) Feleafel, M. N.; Mirdad, Z. M. Hazard and Effects of Pollution by Lead on Vegetable Crops. *J Agric Environ Ethics* **2013**, *26* (3), 547–567. https://doi.org/10.1007/S10806-012-9403-1.

(84) Ghosh, I.; Sun, L.; Xu, M. Q. Zinc Inhibition of Protein Trans-Splicing and Identification of Regions Essential for Splicing and Association of a Split Intein*. *Journal of Biological Chemistry* **2001**, *276* (26), 24051–24058. https://doi.org/10.1074/JBC.M011049200.

(85) Tharappel, A. M.; Li, Z.; Li, H. Inteins as Drug Targets and Therapeutic Tools. *Front Mol Biosci* **2022**, *9*, 821146. https://doi.org/10.3389/FMOLB.2022.821146.

(86) Alhazmi, H. A.; Alam, M. S.; Albratty, M.; Najmi, A.; Abdulhaq, A. A.; Hassani, R.; Ahsan, W.; Qramish, A. N. Binding Investigation of Some Important Metal Ions Copper (I), Nickel (II), and Aluminium (III) with Bovine Serum Albumin Using Valid Spectroscopic Techniques. *J Chem* **2023**, *2023* (1), 2581653. https://doi.org/10.1155/2023/2581653.

(87) Permyakov, E. A.; Gonçalves, A. M. M. Metal Binding Proteins. *Encyclopedia* **2021**, *1* (1), 261–292. https://doi.org/10.3390/ENCYCLOPEDIA1010024.

(88) Woźnicka, O.; Rybarska, J.; Jagusiak, A.; Konieczny, L.; Stopa, B.; Roterman, I. Metal Ions Introduced to Proteins by Supramolecular Ligands. *Self-Assembled Molecules - New Kind of Protein Ligands: Supramolecular Ligands* **2017**, 61–76. https://doi.org/10.1007/978-3-319-65639-7_4.

(89) Antosiewicz, J. M.; Shugar, D. UV–Vis Spectroscopy of Tyrosine Side-Groups in Studies of Protein Structure. Part 2: Selected Applications. *Biophys Rev* **2016**, *8* (2), 163–177. https://doi.org/10.1007/s12551-016-0197-7.

(90) Biter, A. B.; Pollet, J.; Chen, W. H.; Strych, U.; Hotez, P. J.; Bottazzi, M. E. A Method to Probe Protein Structure from UV Absorbance Spectra. *Anal Biochem* **2019**, *587*, 113450. https://doi.org/10.1016/J.AB.2019.113450.

(91) Dieaconu, M.; Ioanid, A.; Iftimie, S.; Antohe, S. UV-ABSORPTION MECHANISMS OF Ni 2+-BINDING BOVINE SERUM ALBUMIN. *Dig J Nanomater Biostruct 7* (3), 1125–1138.

(92) *View of Study of immunoglobulin 'G' with ultra violet spectroscopy in Duchene muscular dystrophy and Alzheimer's disease*. https://journals.scholarpublishing.org/index.php/BJHR/article/view/100/98 (accessed 2025-06-16).

(93) Bjørklund, G.; Dadar, M.; Mutter, J.; Aaseth, J. The Toxicology of Mercury: Current Research and Emerging Trends. *Environ Res* **2017**, *159*, 545–554. https://doi.org/10.1016/J.ENVRES.2017.08.051.

(94) Ajsuvakova, O. P.; Tinkov, A. A.; Aschner, M.; Rocha, J. B. T.; Michalke, B.; Skalnaya, M. G.; Skalny, A. V.; Butnariu, M.; Dadar, M.; Sarac, I.; Aaseth, J.; Bjørklund, G. Sulfhydryl Groups as Targets of Mercury Toxicity. *Coord Chem Rev* **2020**, *417*, 213343. https://doi.org/10.1016/J.CCR.2020.213343.

(95) Sall, M. L.; Diaw, A. K. D.; Gningue-Sall, D.; Efremova Aaron, S.; Aaron, J. J. Toxic Heavy Metals: Impact on the Environment and Human Health, and Treatment with Conducting Organic Polymers, a Review. *Environmental Science and Pollution Research* **2020**, *27* (24), 29927–29942. https://doi.org/10.1007/s11356-020-09354-3.

(96) Gonick, H. C. Lead-Binding Proteins: A Review. *J Toxicol* **2011**, *2011* (1), 686050. https://doi.org/10.1155/2011/686050.

(97) Fossum, C. J.; Johnson, B. O. V.; Golde, S. T.; Kielman, A. J.; Finke, B.; Smith, M. A.; Lowater, H. R.; Laatsch, B. F.; Bhattacharyya, S.; Hati, S. Insights into the Mechanism of Tryptophan Fluorescence Quenching Due to Synthetic Crowding Agents: A Combined Experimental and Computational Study. *ACS Omega* **2023**, *8* (47), 44820–44830. https://doi.org/10.1021/acsomega.3c06006.

(98) Liu, Y.; Xu, J.; Han, L.; Liu, Q.; Yang, Y.; Li, Z.; Lu, Z.; Zhang, H.; Guo, T.; Liu, Q. Theoretical Research on Excited States: Ultraviolet and Fluorescence Spectra of Aromatic Amino Acids. *Interdiscip Sci* **2020**, *12* (4), 530–536. https://doi.org/10.1007/s12539-020-00395-3.

(99) Yammine, A.; Gao, J.; Kwan, A. H. Tryptophan Fluorescence Quenching Assays for Measuring Protein-Ligand Binding Affinities: Principles and a Practical Guide. *Bio Protoc* **2019**, *9* (11). https://doi.org/10.21769/BIOPROTOC.3253.

(100) Zheng, Z.; Kawakami, K.; Zhang, D.; Negishi, L.; Abomosallam, M.; Asakura, T.; Nagata, K.; Suzuki, M. Identification and Functional Analysis of Cadmium-Binding Protein in the Visceral Mass of Crassostrea Gigas. *Sci Rep* **2021**, *11* (1), 1–14. https://doi.org/10.1038/s41598-021-90882-4.

(101) Springfield, E.; Willis, A.; Merle, J.; Mazlo, J.; Ngu-Schwemlein, M. Spectroscopic and Theoretical Studies of Hg(II) Complexation with Some Dicysteinyl Tetrapeptides. *Bioinorg Chem Appl* **2021**, *2021* (1), 9911474. https://doi.org/10.1155/2021/9911474.

(102) Crouse, H. F.; Petrunak, E. M.; Donovan, A. M.; Merkle, A. C.; Swartz, B. L.; Basu, S. Static and Dynamic Quenching of Tryptophan Fluorescence in Various Proteins by a Chromium (III) Complex. *Spectroscopy Letters* **2011**, *44* (5), 369–374. https://doi.org/10.1080/00387010.2010.546470.

(103) Shrivastava, H. Y.; Nair, B. U. Fluorescence Resonance Energy Transfer from Tryptophan to a Chromium(III) Complex Accompanied by Non-Specific Cleavage of Albumin: A Step Forward towards the Development of a Novel Photoprotease. *J Inorg Biochem* **2004**, *98* (6), 991–994. https://doi.org/10.1016/J.JINORGBIO.2004.02.014.

(104) Liu, Y.; Zhang, L.; Liu, R.; Zhang, P. Spectroscopic Identification of Interactions of Pb 2+ with Bovine Serum Albumin. *J Fluoresc* **2012**, *22* (1), 239–245. https://doi.org/10.1007/s10895-011-0950-z.

(105) Gen-hua Wu. *Study on the interaction of Pb2+ and bovine serum albumin by fluorescence*. https://europepmc.org/article/med/15852867 (accessed 2025-06-16).

(106) Luis, G.; Rubio, C.; Revert, C.; Espinosa, A.; González-Weller, D.; Gutiérrez, A. J.; Hardisson, A. Dietary Intake of Metals from Yogurts Analyzed by Inductively Coupled Plasma Optical Emission Spectrometry (ICP-OES). *Journal of Food Composition and Analysis* **2015**, *39*, 48–54. https://doi.org/10.1016/J.JFCA.2014.11.013.

(107) Wiltsche, H.; Wolfgang, M. Merits of Microwave Plasmas for Optical Emission Spectrometry – Characterization of an Axially Viewed Microwave-Sustained, Inductively Coupled, Atmospheric-Pressure Plasma (MICAP). *J Anal At Spectrom* **2020**, *35* (10), 2369–2377. https://doi.org/10.1039/D0JA00293C.

(108) Baraud, F.; Zaiter, A.; Porée, S.; Leleyter, L. New Approach for Determination of Cd, Cu, Cr, Ni, Pb, and Zn in Sewage Sludges, Fired Brick, and Sediments Using Two Analytical Methods by Microwave-Induced Plasma Optical Spectrometry and Induced Coupled Plasma Optical Spectrometry. *SN Appl Sci* **2020**, *2* (9), 1–10. https://doi.org/10.1007/s42452-020-03220-0.

(109) Wegener Antje; Marc Wiesmann; Peter Luschas; Kerstin Vogel; Matthias Pursch. *SEC-ICP-OES Hyphenation: Speciation and Quantification of Polydimethylsiloxanes at Trace levels*. Spectroscopy. https://www.spectroscopyonline.com/view/sec-icp-oes-hyphenation-speciation-and-quantification-polydimethylsiloxanes-trace-levels (accessed 2025-08-01).

1226 (110) Pandey, M.; Talwar, S.; Bose, S.; Pandey, A. K. Iron Homeostasis in Mycobacterium
1227 Tuberculosis Is Essential for Persistence. *Sci Rep* **2018**, *8* (1), 1–9.
1228 https://doi.org/10.1038/S41598-018-35012-3.

1229 (111) Tripathi, A.; Anand, K.; Das, M.; O'Niel, R. A.; Sabarinath, P. S.; Thakur, C.; Reddy, R.
1230 R. L.; Rajmani, R. S.; Chandra, N.; Laxman, S.; Singh, A. Mycobacterium Tuberculosis
1231 Requires SufT for Fe-S Cluster Maturation, Metabolism, and Survival in Vivo. *PLoS*
1232 *Pathog* **2022**, *18* (4), e1010475. https://doi.org/10.1371/JOURNAL.PPAT.1010475.

1233 (112) Saini, V.; Farhana, A.; Glasgow, J. N.; Steyn, A. J. C. Iron Sulfur Cluster Proteins and
1234 Microbial Regulation: Implications for Understanding Tuberculosis. *Curr Opin Chem Biol*
1235 **2012**, *16* (1–2), 45–53. https://doi.org/10.1016/J.CBPA.2012.03.004.

1236 (113) Zhang, L.; Xiao, N.; Pan, Y.; Zheng, Y.; Pan, Z.; Luo, Z.; Xu, X.; Liu, Y. Binding and
1237 Inhibition of Copper Ions to RecA Inteins from Mycobacterium Tuberculosis. *Chemistry –*
1238 *A European Journal* **2010**, *16* (14), 4297–4306.
1239 https://doi.org/10.1002/CHEM.200903584.

1240 (114) Shaloam R, D. Preclinical Assessment of Low Doses of Cisplatin in the Management of
1241 Acute Promyelocytic Leukemia. *Int J Cancer Res Mol Mech* **2015**, *1* (3).
1242 https://doi.org/10.16966/2381-3318.113.

1243 (115) Topilina, N. I.; Green, C. M.; Jayachandran, P.; Kelley, D. S.; Stanger, M. J.; Piazza, C.
1244 L.; Nayak, S.; Belfort, M. SufB Intein of Mycobacterium Tuberculosis as a Sensor for
1245 Oxidative and Nitrosative Stresses. *Proc Natl Acad Sci U S A* **2015**, *112* (33), 10348–
1246 10353. https://doi.org/10.1073/pnas.1512777112.

1247 (116) Lennon, C. W.; Wahl, D.; Goetz, J. R.; Joel Weinberger, I. Reactive Chlorine Species
1248 Reversibly Inhibit DnaB Protein Splicing in Mycobacteria. *Microbiol Spectr* **2021**, *9* (2).
1249 https://doi.org/10.1128/SPECTRUM.00301-21.

1250 (117) Wang, P.; Xu, G.; Qin, L.; Xu, Y.; Li, Y.; Li, R. Cell-Based Biosensors and Its
1251 Application in Biomedicine. *Sens Actuators B Chem* **2005**, *108* (1–2), 576–584.
1252 https://doi.org/10.1016/J.SNB.2004.11.056.

1253 (118) Gupta, N.; Renugopalakrishnan, V.; Liepmann, D.; Paulmurugan, R.; Malhotra, B. D.
1254 Cell-Based Biosensors: Recent Trends, Challenges and Future Perspectives. *Biosens*
1255 *Bioelectron* **2019**, *141*, 111435. https://doi.org/10.1016/J.BIOS.2019.111435.

1256 (119) Perler, F. B. InBase: The Intein Database. *Nucleic Acids Res* **2002**, *30* (1), 383–384.
1257 https://doi.org/10.1093/NAR/30.1.383.

1258 (120) Yakovleva, L.; Shuman, S. Mycobacterium Smegmatis SftH Exemplifies a Distinctive
1259 Clade of Superfamily II DNA-Dependent ATPases with 3′ to 5′ Translocase and Helicase

1260 Activities. *Nucleic Acids Res* **2012**, *40* (15), 7465–7475.
1261 https://doi.org/10.1093/NAR/GKS417.

1262 (121) Ordonez, H.; Shuman, S. Mycobacterium Smegmatis Lhr Is a DNA-Dependent ATPase
1263 and a 3′-to-5′ DNA Translocase and Helicase That Prefers to Unwind 3′-Tailed
1264 RNA:DNA Hybrids. *Journal of Biological Chemistry* **2013**, *288* (20), 14125–14134.
1265 https://doi.org/10.1074/JBC.M113.466854.

1266 (122) Uson, M. L.; Ordonez, H.; Shuman, S. Mycobacterium Smegmatis HelY Is an RNA-
1267 Activated ATPase/DATPase and 3′-to-5′ Helicase That Unwinds 3′-Tailed RNA Duplexes
1268 and RNA:DNA Hybrids. *J Bacteriol* **2015**, *197* (19), 3057–3065.
1269 https://doi.org/10.1128/JB.00418-15.

1270 (123) Rampersad, S. N. Multiple Applications of Alamar Blue as an Indicator of Metabolic
1271 Function and Cellular Health in Cell Viability Bioassays. *Sensors* **2012**, *12* (9), 12347–
1272 12360. https://doi.org/10.3390/S120912347.

1273 (124) O'Brien, J.; Wilson, I.; Orton, T.; Pognan, F. Investigation of the Alamar Blue (Resazurin)
1274 Fluorescent Dye for the Assessment of Mammalian Cell Cytotoxicity. *Eur J Biochem*
1275 **2000**, *267* (17), 5421–5426. https://doi.org/10.1046/j.1432-1327.2000.01606.x.

1276 (125) McMillan, J. E. *Principles of Analytical Validation*; Elsevier Inc., 2013.
1277 https://doi.org/10.1016/B978-0-444-59378-8.00011-6.

1278 (126) Howard, J. A.; Kuznietsova, H.; Dziubenko, N.; Aigle, A.; Natuzzi, M.; Thomas, E.;
1279 Lysenko, V.; David, L.; Brichart, T.; Lux, F.; Tillement, O. Combating Lead and
1280 Cadmium Exposure with an Orally Administered Chitosan-Based Chelating Polymer. *Sci*
1281 *Rep* **2023**, *13* (1), 1–14. https://doi.org/10.1038/s41598-023-28968-4.

1282 (127) Saleh, S. M.; El-Tawil, O. S.; Mahmoud, M. B.; Abd El-Rahman, S. S.; El-Saied, E. M.;
1283 Noshy, P. A. Do Nanoparticles of Calcium Disodium EDTA Minimize the Toxic Effects
1284 of Cadmium in Female Rats? *Biol Trace Elem Res* **2024**, *202* (5), 2228–2240.
1285 https://doi.org/10.1007/s12011-023-03842-6.

1286 (128) Flora, S. J. S.; Pachauri, V. Chelation in Metal Intoxication. *Int J Environ Res Public*
1287 *Health* **2010**, *7* (7), 2745–2788. https://doi.org/10.3390/IJERPH7072745.

1288 (129) Bethesda. *LiverTox*; National Institute of Diabetes and Digestive and Kidney Diseases,
1289 2012.

1290 (130) George, G. N.; Prince, R. C.; Gailer, J.; Buttigieg, G. A.; Denton, M. B.; Harris, H. H.;
1291 Pickering, I. J. Mercury Binding to the Chelation Therapy Agents DMSA and DMPS and
1292 the Rational Design of Custom Chelators for Mercury. *Chem Res Toxicol* **2004**, *17* (8),
1293 999–1006. https://doi.org/10.1021/tx049904e.

1294 (131) Aaseth, J.; Ajsuvakova, O. P.; Skalny, A. V.; Skalnaya, M. G.; Tinkov, A. A. Chelator
1295 Combination as Therapeutic Strategy in Mercury and Lead Poisonings. *Coord Chem Rev*
1296 **2018**, *358*, 1–12. https://doi.org/10.1016/J.CCR.2017.12.011.

1297 (132) Martí-Baena, Q.; Pascuet-Fontanet, A.; Berjaga-Buisan, T.; Caravaca-Rodríguez, M.;
1298 Puig-Costa-Jussà, J.; Sanchez-Mejias, A.; Ivančić, D.; Mogas-Díez, S.; Güell, M.; Macia,
1299 J. Intein-Mediated Thyroid Hormone Biosensors: Towards Controlled Delivery of
1300 Hormone Therapy. *Frontiers in Systems Biology* **2024**, *4*, 1270071.
1301 https://doi.org/10.3389/FSYSB.2024.1270071.

1302 (133) Chahal, H. K.; Dai, Y.; Saini, A.; Ayala-Castro, C.; Outten, F. W. The SufBCD Fe−S
1303 Scaffold Complex Interacts with SufA for Fe−S Cluster Transfer. *Biochemistry* **2009**, *48*
1304 (44), 10644–10653. https://doi.org/10.1021/BI901518Y.

1305 (134) Dillon, N. A.; Lamont, E. A.; Rather, M. A.; Baughn, A. D. Oxidative Stress Drives
1306 Potent Bactericidal Activity of Pyrazinamide against Mycobacterium Tuberculosis. *Elife*
1307 **2025**, *14*. https://doi.org/10.7554/ELIFE.105614.1.

1308 (135) Zhang, M.; Gong, J.; Lin, Y.; Barnes, P. F. Growth of Virulent and
1309 AvirulentMycobacterium Tuberculosis Strains in Human Macrophages. *Infect Immun*
1310 **1998**, *66* (2), 794–799. https://doi.org/10.1128/IAI.66.2.794-799.1998.

1311 (136) *Revised National TB Control Programme Training Manual for Mycobacterium*
1312 *tuberculosis*.

1313 (137) Davis, E. O.; Sedgwick, S. G.; Colston, M. J. Novel Structure of the RecA Locus of
1314 Mycobacterium Tuberculosis Implies Processing of the Gene Product. *J Bacteriol* **1991**,
1315 *173* (18), 5653–5662. https://doi.org/10.1128/JB.173.18.5653-5662.1991.

1316 (138) Saves, I.; Westrelin, F.; Daffé, M.; Masson, J. M. Identification of the First Eubacterial
1317 Endonuclease Coded by an Intein Allele in the Pps1 Gene of Mycobacteria. *Nucleic Acids*
1318 *Res* **2001**, *29* (21), 4310–4318. https://doi.org/10.1093/NAR/29.21.4310.

1319 (139) Schneider, R. F.; Hallstrom, K.; DeMott, C.; McDonough, K. A. Conditional Protein
1320 Splicing of the Mycobacterium Tuberculosis RecA Intein in Its Native Host. *Sci Rep*
1321 **2024**, *14* (1), 1–14. https://doi.org/10.1038/S41598-024-71248-Y.

1322

1323

A.

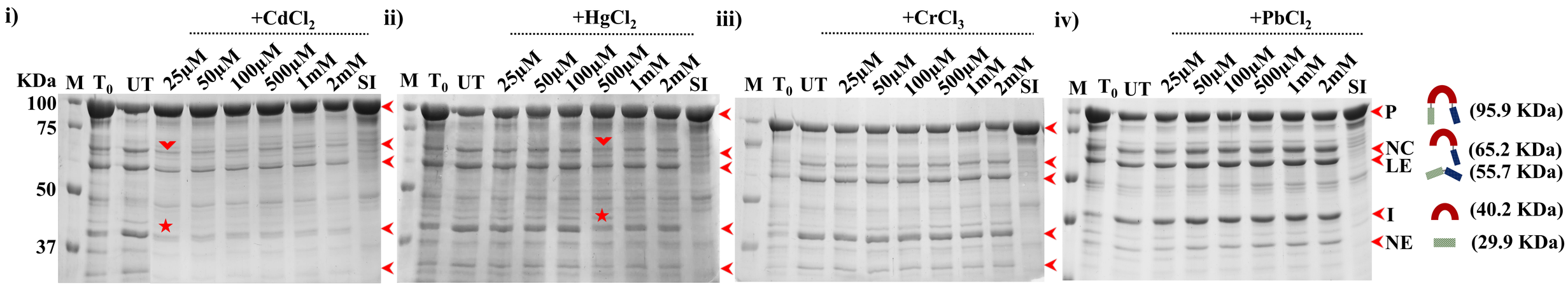
i)
+CdCl2
ii)
+HgCl2
iii)
+CrCl3
iv)
+PbCl2
KDa
M T0 UT 25µM 50µM 100µM 500µM 1mM 2mM SI
100
75
50
37
P
NC
LE
I
NE
(95.9 KDa)
(65.2 KDa)
(55.7 KDa)
(40.2 KDa)
(29.9 KDa)

B.

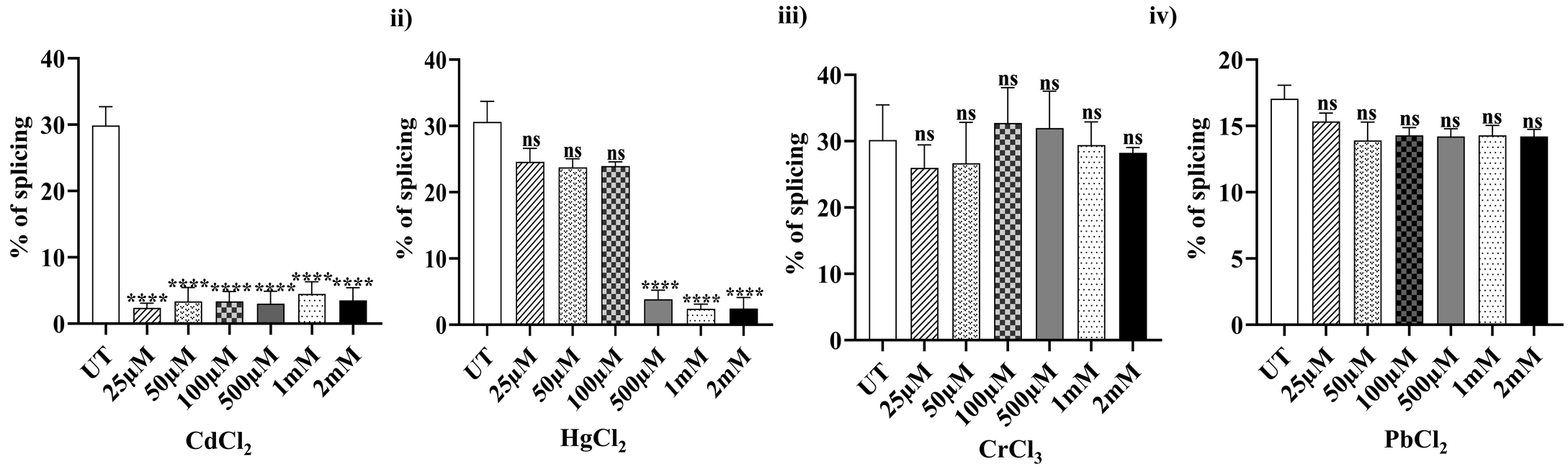
i)
ii)
iii)
iv)
% of splicing
UT 25µM 50µM 100µM 500µM 1mM 2mM
CdCl2
HgCl2
CrCl3
PbCl2
****
ns

C.

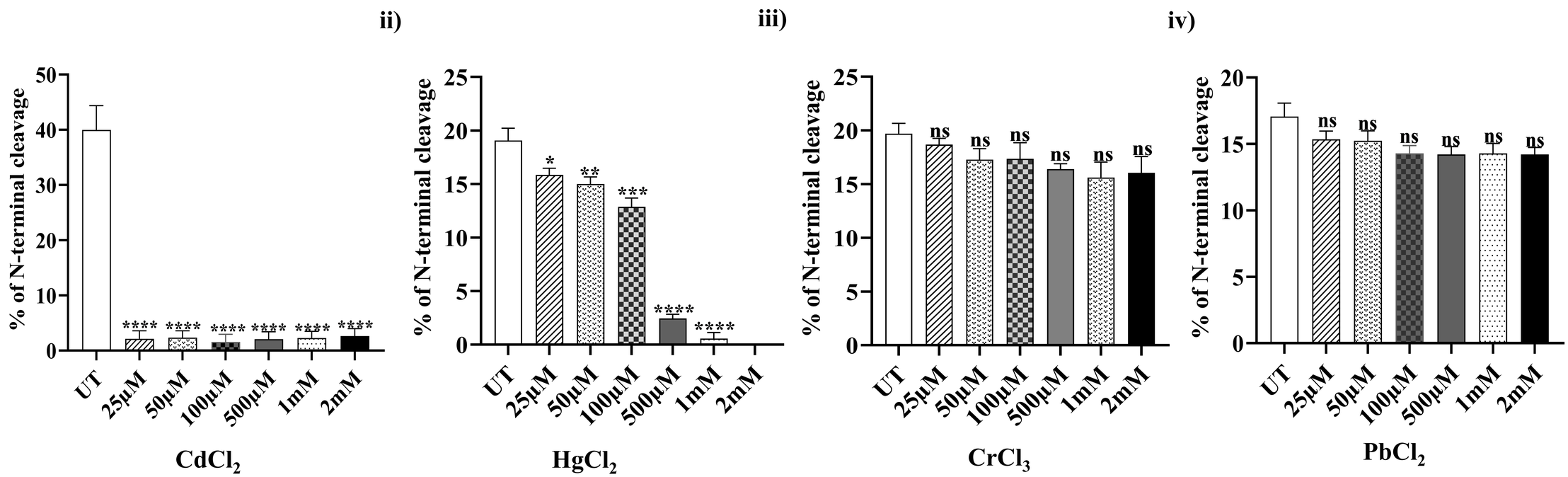
i)
ii)
iii)
iv)
% of N-terminal cleavage
UT 25µM 50µM 100µM 500µM 1mM 2mM
CdCl2
HgCl2
CrCl3
PbCl2
****
*
**
***
ns

i)

Cd^{2+} | Hg^{2+}

H37Ra | *M. sm* | H37Ra | *M. sm*

Cd 2.5 µM	Cd 25 µM	Cd 100 µM	Cd 1 mM	*M.Sm* +Cd 25 µM	Hg 25 µM	Hg 100 µM	Hg 1 mM	*M.Sm* + Hg 25 µM	+ve control
Cd 2.5 µM	Cd 25 µM	Cd 100 µM	Cd 1 mM	*M.Sm* +Cd 25 µM	Hg 25 µM	Hg 100 µM	Hg 1 mM	*M.Sm* + Hg 25 µM	+ve control
Cd 5 µM	Cd 25 µM	Cd 100 µM	Cd 1 mM	*M.Sm* +Cd 500 µM	Hg 25 µM	Hg 100 µM	Hg 1 mM	*M.Sm* +Hg 500 µM	+ve control
Cd 5 µM	Cd 50 µM	Cd 500 µM	Cd 2 mM	*M.Sm* +Cd 500 µM	Hg 50 µM	Hg 500 µM	Hg 2 mM	*M.Sm* +Hg 500 µM	-ve control
Cd 10 µM	Cd 50 µM	Cd 500 µM	Cd 2 mM	*M.Sm* +Cd 2 mM	Hg 50 µM	Hg 500 µM	Hg 2 mM	*M.Sm* + Hg 2 mM	-ve control
Cd 10 µM	Cd 50 µM	Cd 500 µM	Cd 2 mM	*M.Sm* +Cd 2 mM	Hg 50 µM	Hg 500 µM	Hg 2 mM	*M.Sm* + Hg 2 mM	-ve control

+ve control

-ve control

ii)

Cd^{2+} | Hg^{2+}

H37Ra | *M. sm* | H37Ra | *M. sm*

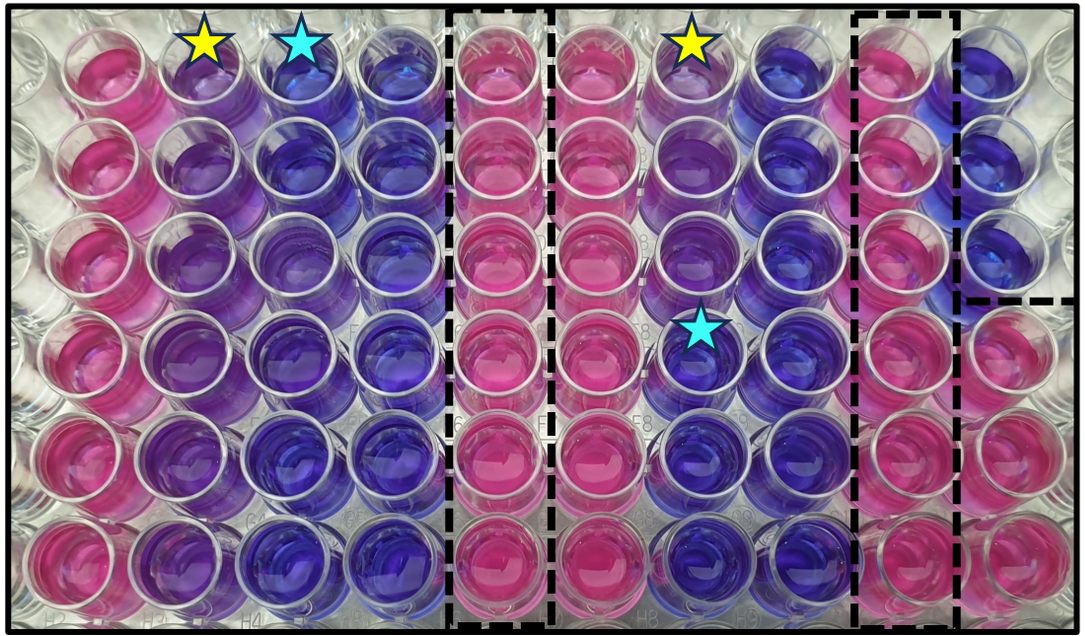

+ve control

-ve control

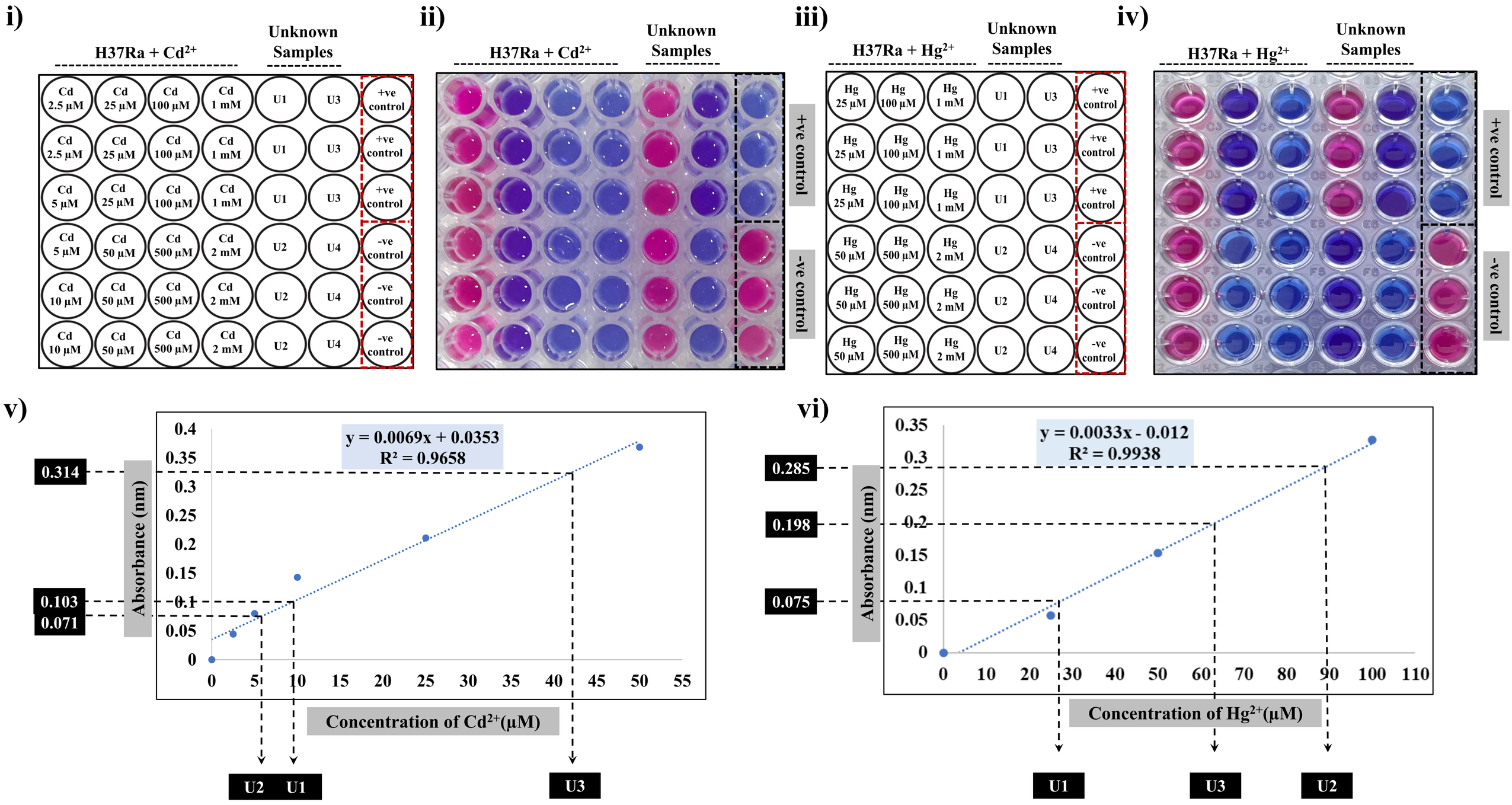
i)
H37Ra + Cd2+
Unknown Samples
Cd 2.5 µM
Cd 25 µM
Cd 100 µM
Cd 1 mM
U1
U3
+ve control
Cd 5 µM
Cd 50 µM
Cd 500 µM
Cd 2 mM
U2
U4
-ve control
Cd 10 µM
ii)
H37Ra + Cd2+
Unknown Samples
+ve control
-ve control
iii)
H37Ra + Hg2+
Unknown Samples
Hg 25 µM
Hg 100 µM
Hg 1 mM
Hg 50 µM
Hg 500 µM
Hg 2 mM
iv)
H37Ra + Hg2+
Unknown Samples
+ve control
-ve control
v)
y = 0.0069x + 0.0353
R² = 0.9658
Absorbance (nm)
0.314
0.103
0.071
Concentration of Cd2+(µM)
U2
U1
U3
vi)
y = 0.0033x - 0.012
R² = 0.9938
Absorbance (nm)
0.285
0.198
0.075
Concentration of Hg2+(µM)
U1
U3
U2

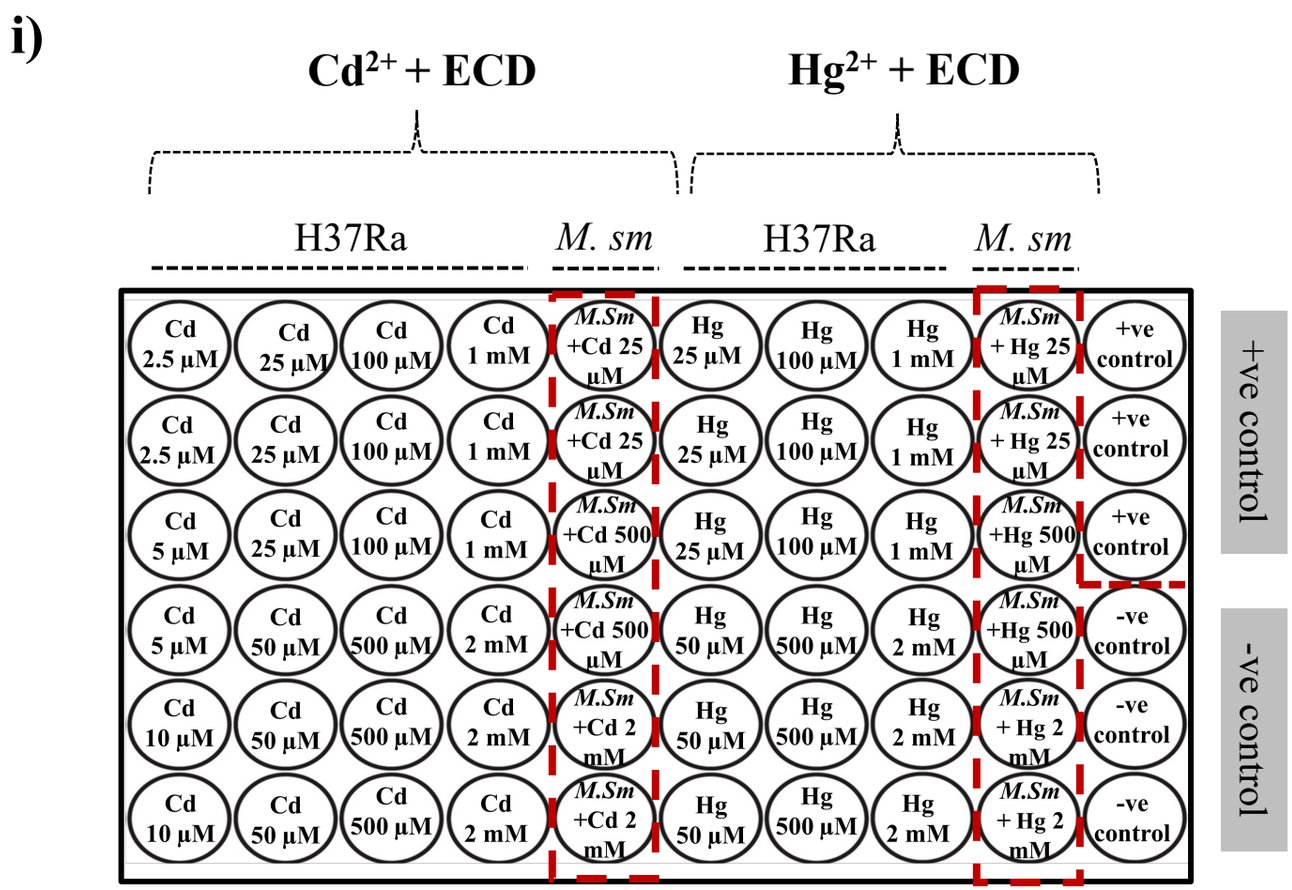
i)
Cd2+ + ECD
Hg2+ + ECD
H37Ra
M. sm
H37Ra
M. sm
Cd 2.5 µM
Cd 25 µM
Cd 100 µM
Cd 1 mM
M.Sm +Cd 25 µM
Hg 25 µM
Hg 100 µM
Hg 1 mM
M.Sm + Hg 25 µM
+ve control
Cd 5 µM
Cd 50 µM
Cd 500 µM
Cd 2 mM
M.Sm +Cd 500 µM
Hg 50 µM
Hg 500 µM
Hg 2 mM
M.Sm +Hg 500 µM
-ve control
Cd 10 µM
M.Sm +Cd 2 mM
M.Sm + Hg 2 mM
+ve control
-ve control

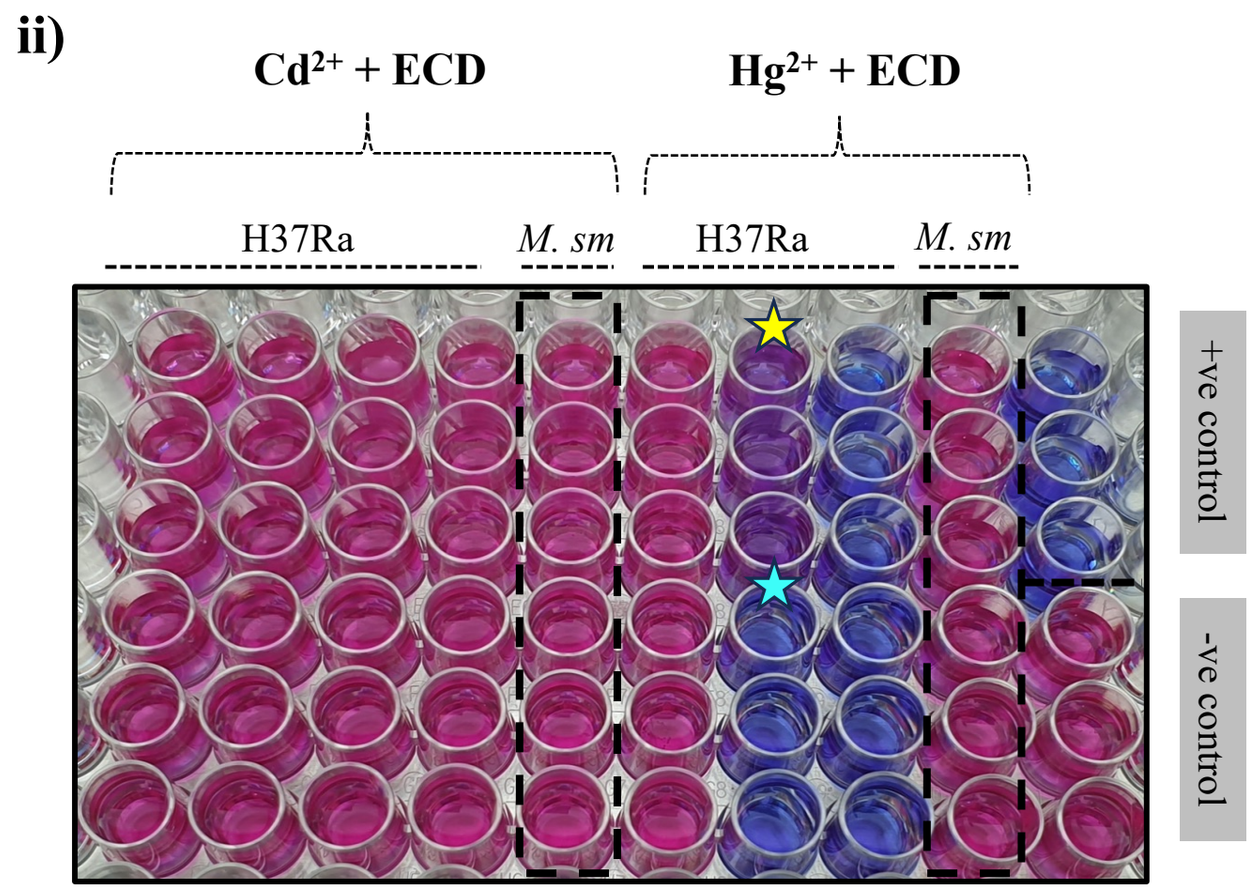
ii)
Cd2+ + ECD
Hg2+ + ECD
H37Ra
M. sm
H37Ra
M. sm
+ve control
-ve control

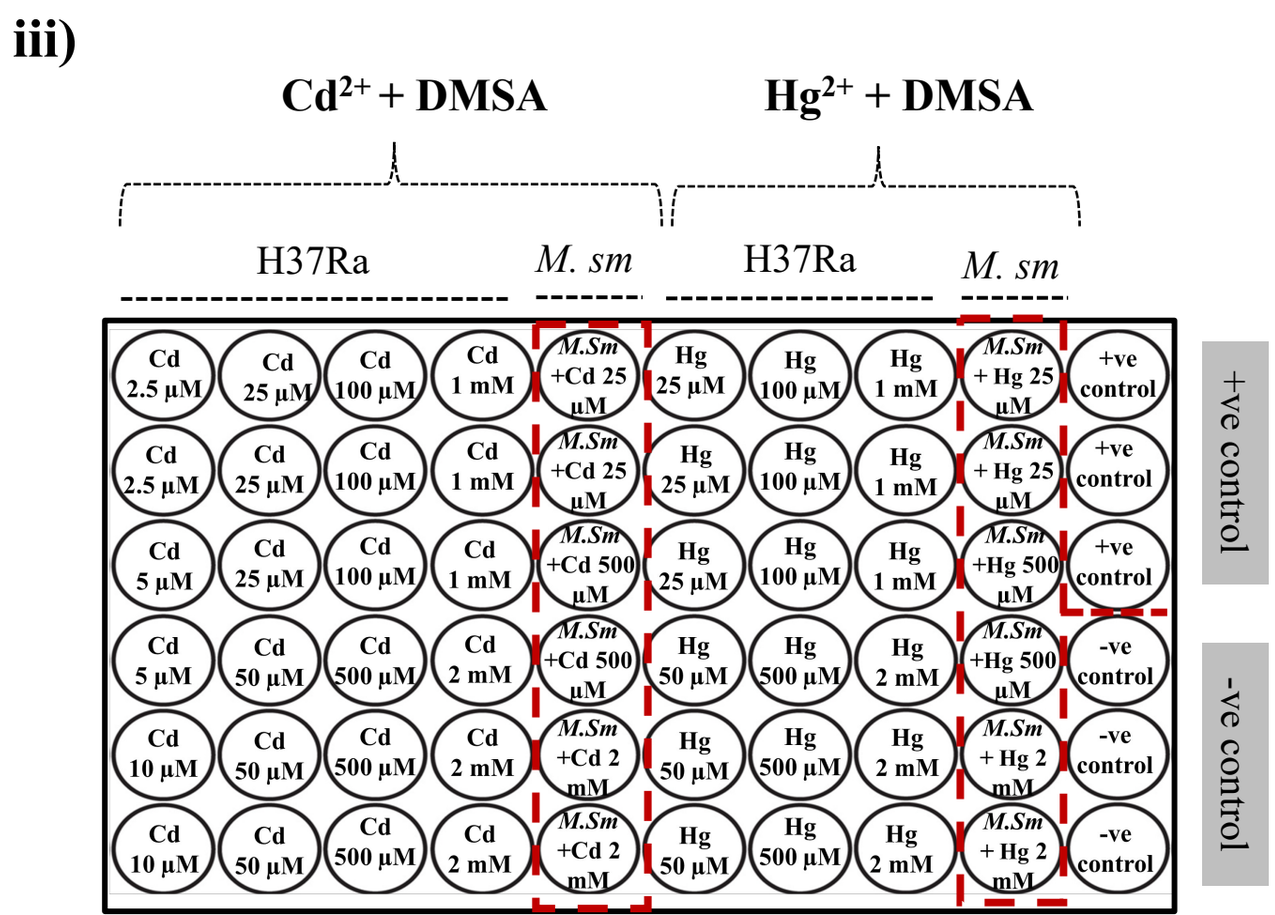
iii)
Cd2+ + DMSA
Hg2+ + DMSA
H37Ra
M. sm
H37Ra
M. sm
Cd 2.5 µM
Cd 25 µM
Cd 100 µM
Cd 1 mM
M.Sm +Cd 25 µM
Hg 25 µM
Hg 100 µM
Hg 1 mM
M.Sm + Hg 25 µM
+ve control
Cd 5 µM
Cd 50 µM
Cd 500 µM
Cd 2 mM
M.Sm +Cd 500 µM
Hg 50 µM
Hg 500 µM
Hg 2 mM
M.Sm +Hg 500 µM
-ve control
Cd 10 µM
M.Sm +Cd 2 mM
M.Sm + Hg 2 mM
+ve control
-ve control

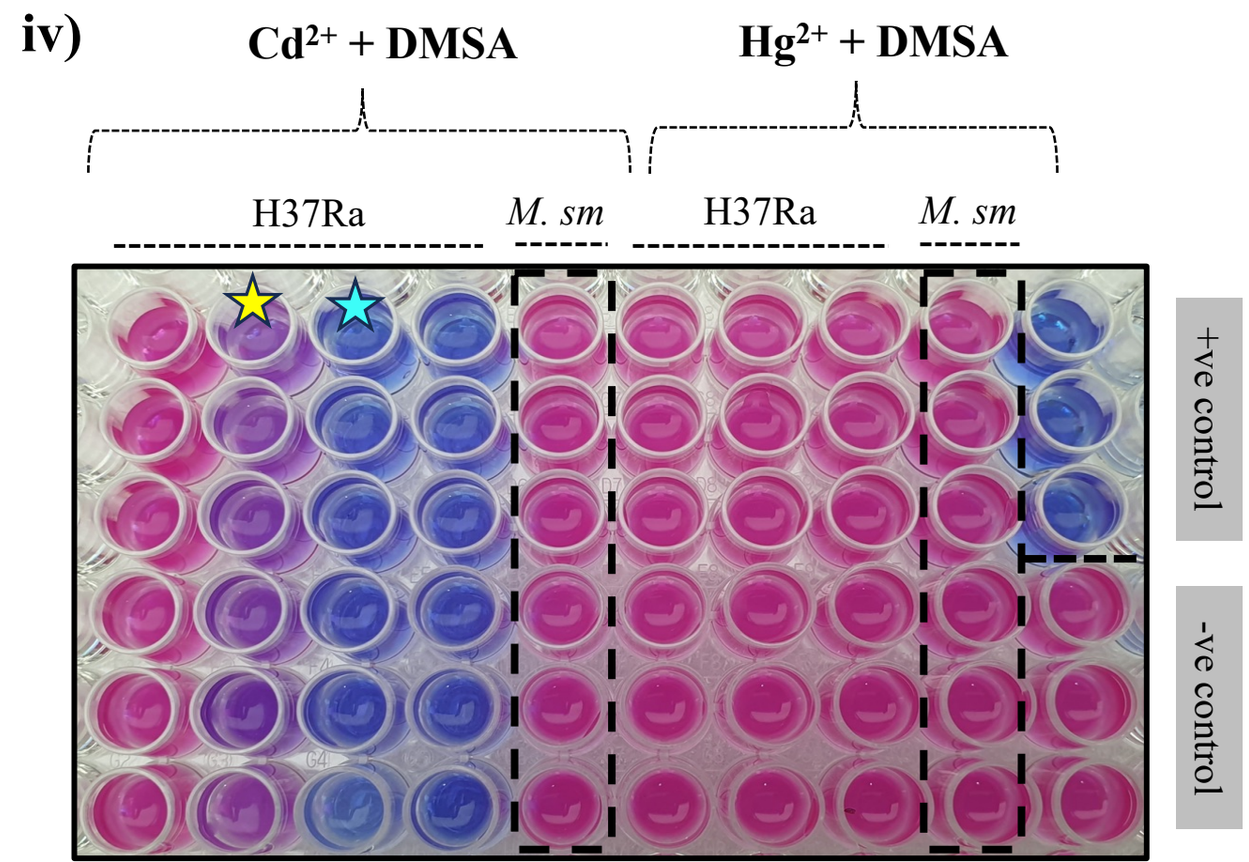
iv)
Cd2+ + DMSA
Hg2+ + DMSA
H37Ra
M. sm
H37Ra
M. sm
+ve control
-ve control

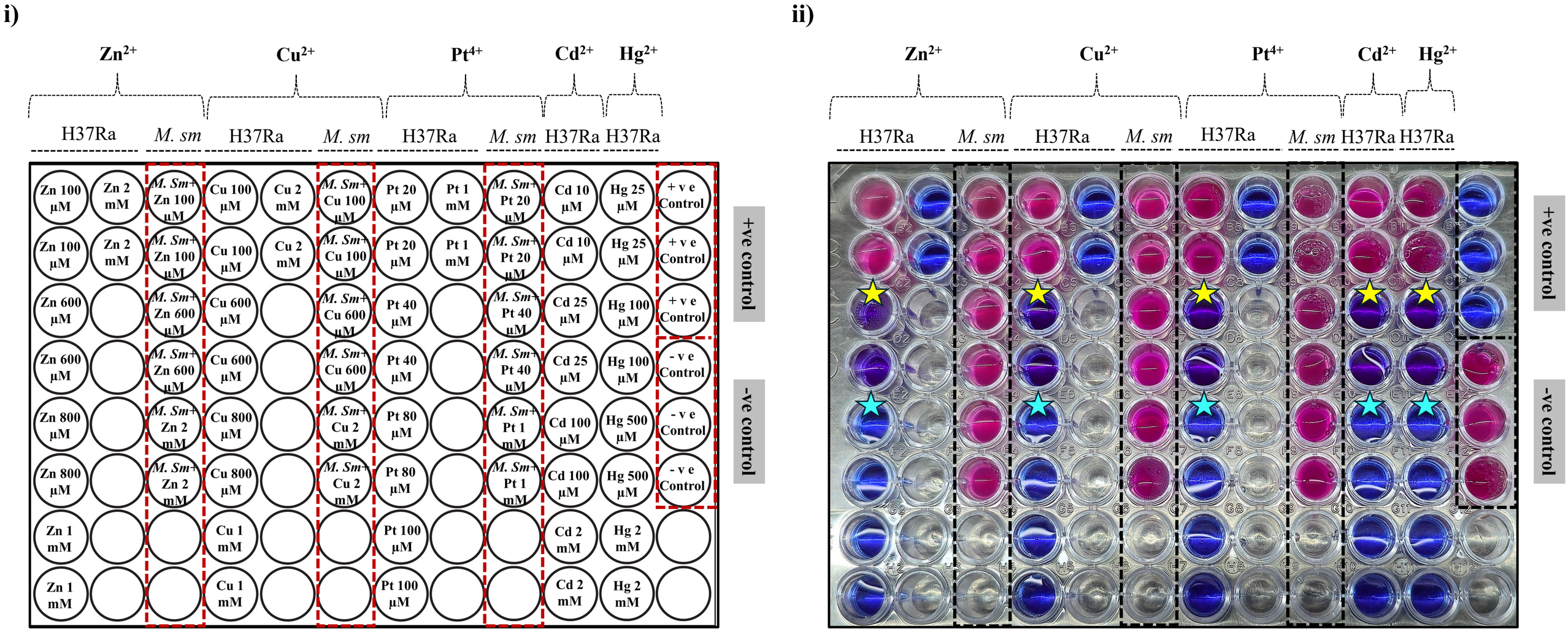
i)
Zn2+
Cu2+
Pt4+
Cd2+
Hg2+
H37Ra
M. sm
H37Ra
M. sm
H37Ra
M. sm
H37Ra
H37Ra
Zn 100 µM
Zn 2 mM
M. Sm+ Zn 100 µM
Cu 100 µM
Cu 2 mM
M. Sm+ Cu 100 µM
Pt 20 µM
Pt 1 mM
M. Sm+ Pt 20 µM
Cd 10 µM
Hg 25 µM
+ v e Control
Zn 100 µM
Zn 2 mM
M. Sm+ Zn 100 µM
Cu 100 µM
Cu 2 mM
M. Sm+ Cu 100 µM
Pt 20 µM
Pt 1 mM
M. Sm+ Pt 20 µM
Cd 10 µM
Hg 25 µM
+ v e Control
Zn 600 µM
M. Sm+ Zn 600 µM
Cu 600 µM
M. Sm+ Cu 600 µM
Pt 40 µM
M. Sm+ Pt 40 µM
Cd 25 µM
Hg 100 µM
+ v e Control
Zn 600 µM
M. Sm+ Zn 600 µM
Cu 600 µM
M. Sm+ Cu 600 µM
Pt 40 µM
M. Sm+ Pt 40 µM
Cd 25 µM
Hg 100 µM
- v e Control
Zn 800 µM
M. Sm+ Zn 2 mM
Cu 800 µM
M. Sm+ Cu 2 mM
Pt 80 µM
M. Sm+ Pt 1 mM
Cd 100 µM
Hg 500 µM
- v e Control
Zn 800 µM
M. Sm+ Zn 2 mM
Cu 800 µM
M. Sm+ Cu 2 mM
Pt 80 µM
M. Sm+ Pt 1 mM
Cd 100 µM
Hg 500 µM
- v e Control
Zn 1 mM
Cu 1 mM
Pt 100 µM
Cd 2 mM
Hg 2 mM
Zn 1 mM
Cu 1 mM
Pt 100 µM
Cd 2 mM
Hg 2 mM
+ve control
-ve control
ii)
Zn2+
Cu2+
Pt4+
Cd2+
Hg2+
H37Ra
M. sm
H37Ra
M. sm
H37Ra
M. sm
H37Ra
H37Ra
+ve control
-ve control

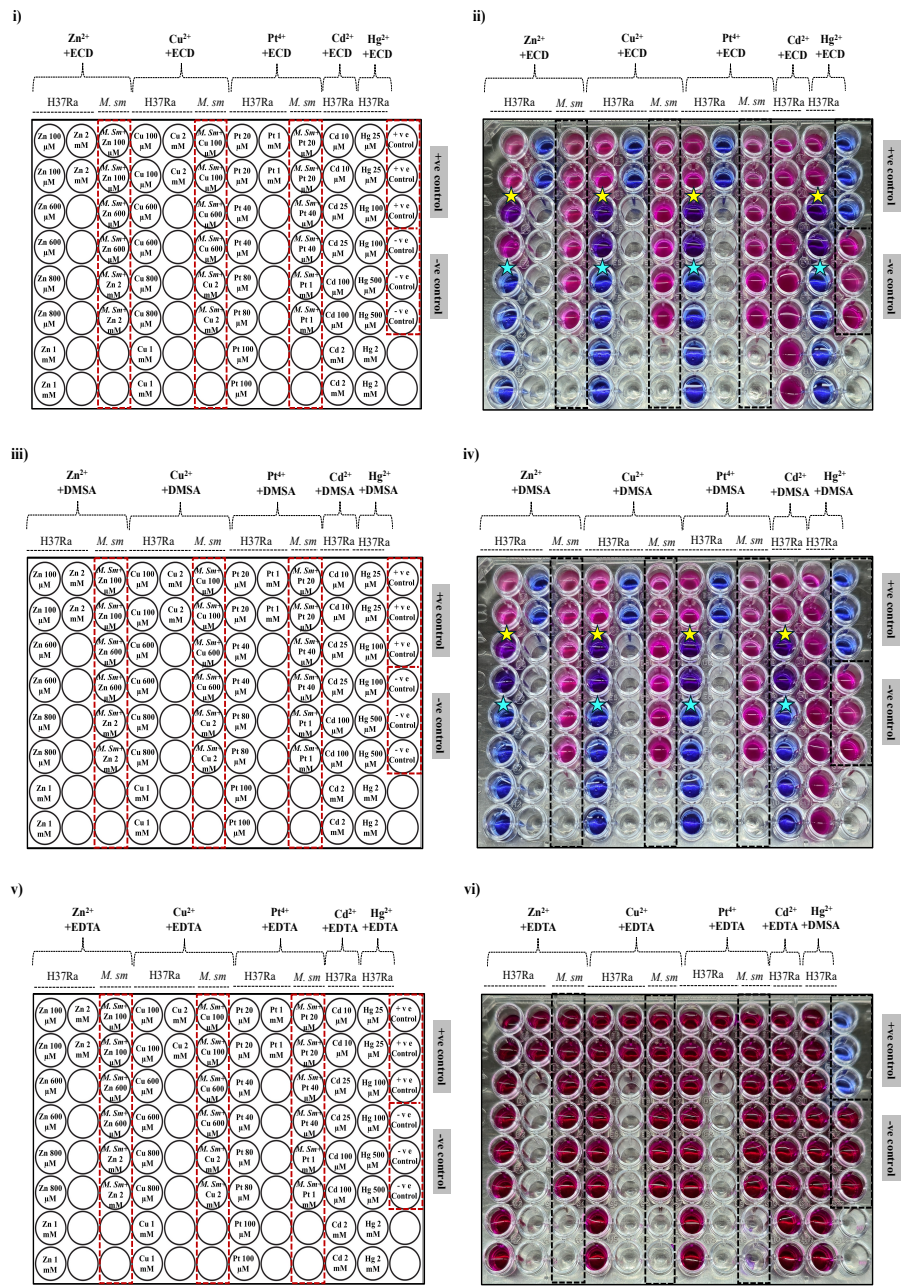
i)
Zn2+ +ECD
Cu2+ +ECD
Pt4+ +ECD
Cd2+ +ECD
Hg2+ +ECD
H37Ra
M. sm
+ve control
-ve control
ii)
iii)
Zn2+ +DMSA
Cu2+ +DMSA
Pt4+ +DMSA
Cd2+ +DMSA
Hg2+ +DMSA
iv)
v)
Zn2+ +EDTA
Cu2+ +EDTA
Pt4+ +EDTA
Cd2+ +EDTA
Hg2+ +EDTA
vi)
Hg2+ +DMSA

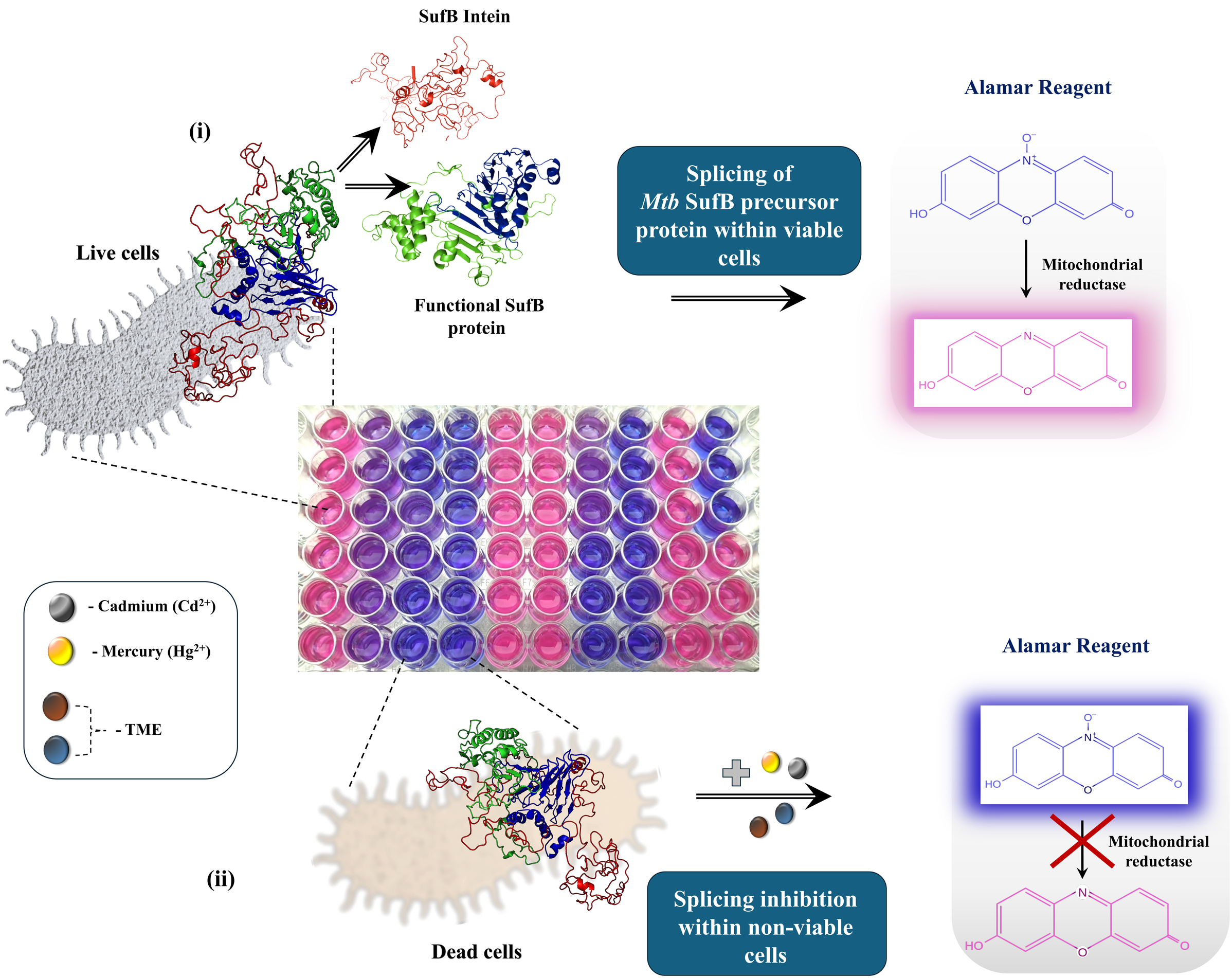
SufB Intein
(i)
Live cells
Functional SufB protein
Splicing of *Mtb* SufB precursor protein within viable cells
Alamar Reagent
Mitochondrial reductase
- Cadmium (Cd^{2+})
- Mercury (Hg^{2+})
- TME
(ii)
Dead cells
Splicing inhibition within non-viable cells
Alamar Reagent
Mitochondrial reductase